

Bioorganic & Medicinal Chemistry

Discovery of novel class of histone deacetylase inhibitors as potential anticancer agents

Raafat El-Awady ^{a,b,*}, Ekram Saleh ^c, Rifat Hamoudi ^{a,d}, Wafaa S. Ramadan ^{a,d},
Ralph Mazitschek ^e, Manal A. Nael ^{f,g}, Khaled M. Elokely ^g, Magid Abou-Gharbia ^h,
Wayne E. Childers ^h, Vunnam Srinivasulu ^a, Lujain Aloum ⁱ, Varsha Menon ^a, Taleb H. Al-Tel ^{a,b,*}

^a Sharjah Institute for Medical Research, University of Sharjah, Sharjah 27272, United Arab Emirates

^b College of Pharmacy, University of Sharjah, Sharjah 27272, United Arab Emirates

^c Cancer Biology Department, National Cancer Institute, Cairo University, Cairo 11796, Egypt

^d College of Medicine, University of Sharjah, Sharjah 27272, United Arab Emirates

^e Center for Systems Biology, Massachusetts General Hospital, Boston, MA 02114, United states

^f Department of Pharmaceutical Chemistry, Faculty of Pharmacy, Tanta University, Tanta 31527, Egypt

^g Institute for Computational Molecular Science, and Department of Chemistry, Temple University, Philadelphia, PA 19122, United States

^h Moulder Center for Drug Discovery Research, Department of Pharmaceutical Sciences, School of Pharmacy, Temple University, Philadelphia, PA 19122, United States

ⁱ Department of Pharmacology, College of Medicine and Health Sciences, Khalifa University of Science and Technology, Abu Dhabi 127788, United Arab Emirates

ARTICLE INFO

Keywords:

Histone deacetylase inhibitors
Anticancer
Cell cycle
Apoptosis
Transcriptomic
Imidazopyridines
Multicomponent reactions
Groebke-Blackburn-Bienayme' reaction

ABSTRACT

Selective inhibition of histone deacetylases (HDACs) is an important strategy in the field of anticancer drug discovery. However, lack of inhibitors that possess high selectivity toward certain HDACs isozymes is associated with adverse side effects that limits their clinical applications. We have initiated a collaborative initiatives between multi-institutions aimed at the discovery of novel and selective HDACs inhibitors. To this end, a phenotypic screening of an in-house pilot library of about 70 small molecules against various HDAC isozymes led to the discovery of five compounds that displayed varying degrees of HDAC isozyme selectivity. The anticancer activities of these molecules were validated using various biological assays including transcriptomic studies. Compounds **15**, **14**, and **19** possessed selective inhibitory activity against HDAC5, while **28** displayed selective inhibition of HDAC1 and HDAC2. Compound **22** was found to be a selective inhibitor for HDAC3 and HDAC9. Importantly, we discovered a none-hydroxamate based HDAC inhibitor, compound **28**, representing a distinct chemical probe of HDAC inhibitors. It contains a trifluoromethyloxadiazolyl moiety (TFMO) as a non-chelating metal-binding group. The new compounds showed potent anti-proliferative activity when tested against MCF7 breast cancer cell line, as well as increased acetylation of histones and induce cells apoptosis. The new compounds apoptotic effects were validated through the upregulation of proapoptotic proteins caspases3 and 7 and downregulation of the antiapoptotic biomarkers C-MYC, BCL2, BCL3 and NFκB genes. Furthermore, the new compounds arrested cell cycle at different phases, which was confirmed through downregulation of the CDK1, 2, 4, 6, E2F1 and RB1 proteins. Taken together, our findings provide the foundation for the development of new chemical probes as potential lead drug candidates for the treatment of cancer.

1. Introduction

The classification of HDACs is grouped based on homology to yeast enzymes. This approach yields four distinct classes that vary in size and function. Class I (HDAC1, HDAC2, HDAC3 and HDAC8), class IIa (HDAC4, HDAC5, HDAC7 and HDAC9), class IIb (HDAC6 and HDAC10) and class IV (HDAC11) HDACs contain predicted zinc-dependent

deacetylase domains. The class III proteins form a structurally and mechanistically distinct class of NAD⁺-dependent hydrolases (sirtuins, Sirt1–Sirt7)^{1–5}. Modification of chromatin structure through post-translational histone processes plays a key role in carcinogenesis and has been exploited as an anti-cancer drug discovery mechanism for over a decade^{1–2}. Methylation and acetylation are among the most important routes of post-translational modifications of histones that affect

* Corresponding authors at: College of Pharmacy and Sharjah Institute for Medical Research, University of Sharjah, Sharjah 27272, United Arab Emirates.

E-mail addresses: relawady@sharjah.ac.ae (R. El-Awady), taltal@sharjah.ac.ae (T.H. Al-Tel).

cancerous and normal cells epigenetics³. The acetylation of histones is controlled by two families of enzymes; histone acetyltransferases (HATs) that enhance acetylation, and histone deacetylases (HDACs) that remove histones acetyl groups⁴⁻⁵. Hyper-acetylated histones lead to an open chromatin structure and higher cellular transcriptional activities. Additionally, opened chromatin structure allows the cellular DNA to be more accessible to DNA damaging agents such as anticancer drugs. These findings have encouraged researchers to design compounds that modulate the degree of histone acetylation by altering the function of HATs and/or HDACs.

Abnormal expression of HDACs is present in many diseases including cancer, diabetes, cystic fibrosis, cardiac, pulmonary diseases, inflammatory and neurological disorders⁶. Selective HDAC3 inhibitors have been described as promising agents for the treatment of inflammation and Type 2 diabetes⁷. Furthermore, selective inhibitors of HDAC1 and

HDAC2 have been reported as an effective approach in the management of sickle cell disease⁸.

Despite the discovery of many novel and first-in-class HDACs inhibitors, the toolbox of chemical probes is still lacking potent and selective HDACs inhibitors. This gap originates from the argued catalytic activity of these enzymes but also most likely due to the unfavorable pharmacokinetics and pharmacodynamics parameters of hydroxamate-containing compounds. The latter represents the warhead of many of the HDACs inhibitors. Their low bioavailability and selectivity profiles (multiple off-target interactions) are considered serious concerns during drug development of these molecules⁹⁻¹². Furthermore, due to the strong interaction between a hydroxamate and the zinc metal, target selectivity becomes a considerable challenge in the ability to design potent inhibitors for HDACs that are zinc-based metalloenzyme. Therefore, the discovery of novel metal-chelating or none-chelating

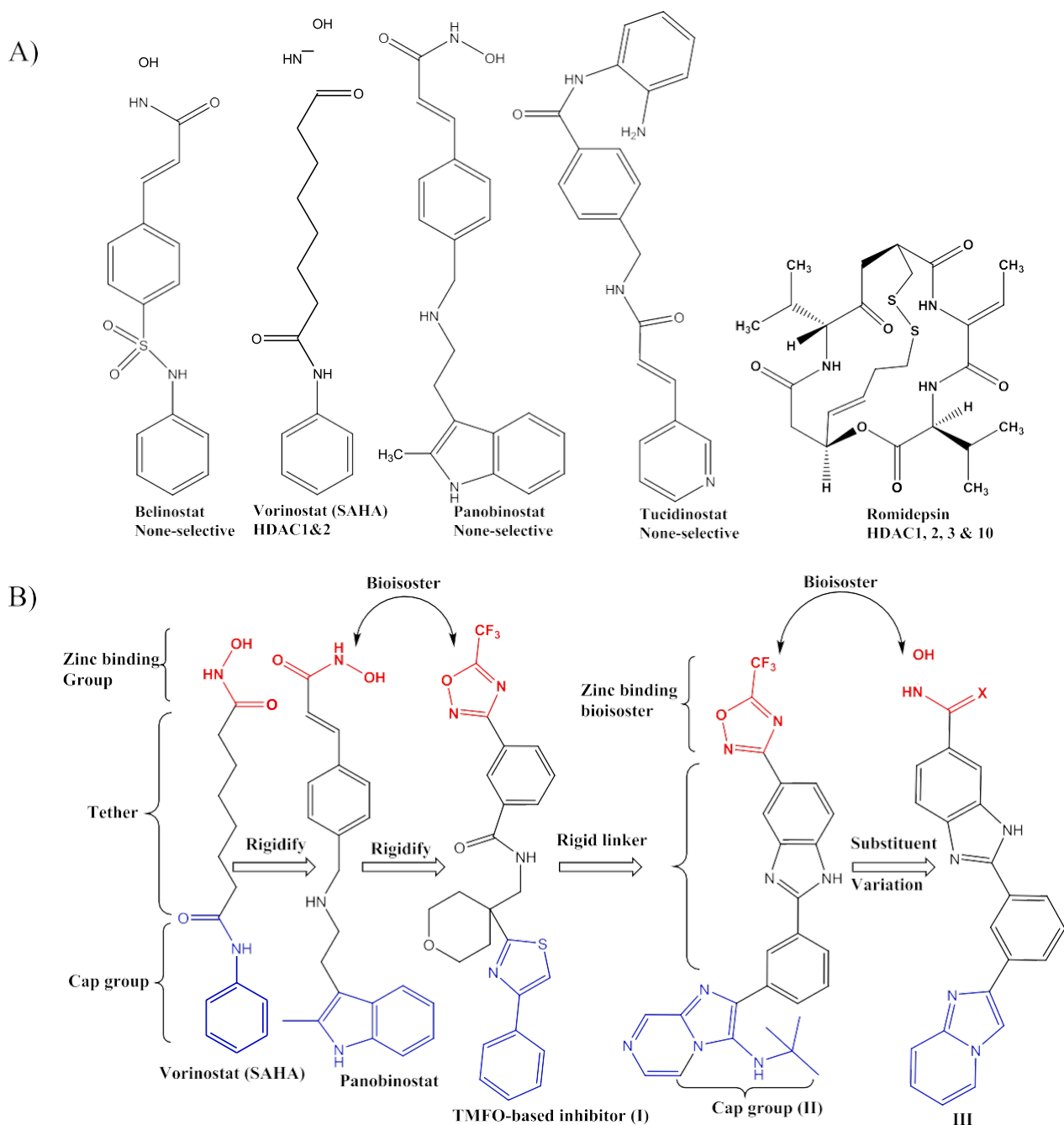


Fig. 1. (A) Representative examples of HDACs inhibitors (B) HDAC inhibitor scaffolds and design strategies.

functional groups is a remarkable achievement¹³. To this end, our group have discovered a distinct series of class IIa HDAC inhibitors containing a trifluoromethyloxadiazolyl moiety (TFMO) as a nonchelating metal-binding group. These novel chemical probes are considered important tools in the HDAC inhibitor field, creating an opportunity to decipher selective inhibitors of these enzymes.

The FDA has approved four histone deacetylase inhibitors (HDACi) for treatment of hematologic and solid malignancies, while many others are in clinical trials, either as a single modality or in combination with other chemotherapeutic drugs^{9–12}. The four FDA-approved drugs include the hydroxamic acid derivatives vorinostat, belinostat and panobinostat and the natural product-derived romidepsin (Fig. 1A). In addition, the benzamide derivative chidamide is approved for treatment of T-cell lymphomas in China and is under clinical review in several other countries. However, these inhibitors suffer from multiple side effects due to the lack of selectivity for therapeutic HDACs over other HDACs involved in normal physiological processes.^{9–12} To overcome these challenges, the development of selective HDAC inhibitors has become an important goal in drug design^{8–10}.

In this article we report the discovery of a new class of selective HDAC inhibitors. The novel structural scaffolds were discovered through an *in vitro* screening campaign of an in-house small molecules collections against various HDAC isozymes. The screening campaign began by first testing around 20 compounds, representing various types of scaffolds, against HDACs1 & 2. Then when hits were discovered, the pilot library representing the scaffold of the best hits were then screened against the other HDACs described in this article. In total, around 70 compounds were screened against the various HDACs isozymes. This process identified five novel molecules that potently inhibit various HDACs, with HDAC selectivity controlled by the substitution pattern on the core scaffold¹³. This new class of HDAC inhibitors possesses an imidazopyridine moiety, which, to the best of our knowledge, has not been reported before. The inhibition of various HDACs by these compounds as well as their effects on acetylated histones, pro-apoptotic and antiapoptotic markers, cell cycle and anti-proliferative activity in the MCF7 breast cancer cell line were investigated^{14–16} and are reported herein.

2. Material and methods

2.1. Biology

2.1.1. Cell line and culture condition

MCF7 cells was purchased from American Type Culture Collection (ATCC, USA) and were preserved in Roswell Park Memorial Institute Medium (RPMI-1640 Gibco, USA) supplemented with 10% fetal bovine serum (Gibco, USA) and penicillin/streptomycin (Gibco, USA). Incubation was performed at 37 °C in a humidified atmosphere of 5% CO₂.

2.1.2. Biochemical HDAC assay

The effect of compounds on HDAC1–HDAC9 enzymes was carried out *in vitro* using an optimized homogenous assay performed in 384-well plate format as previously reported¹⁷. In brief, reactions were performed in assay buffer (50 mM HEPES, 100 mM KCl, 0.001% (v/v) Tween-20, 0.05% (w/v) bovine serum albumin, 200 μM tris(2-carboxyethyl) phosphine (TCEP), pH 7.4) and followed for fluorogenic release of 7-amino-4-methylcoumarin from substrate upon deacetylase and trypsin enzymatic activity. Fluorescence measurements were obtained approximately every 5 min using an Envision multi-label plate reader and plate stacker (Perkin-Elmer, USA). Data were analyzed on a plate-by-plate basis for the linear range of fluorescence over time. The first derivative of data obtained from the plate capture corresponding to the mid-linear range was imported into analytical software (Spotfire DecisionSite and GraphPad Prism). Data was analyzed using logistic regression with calculation of IC₅₀ and s.d. (Spotfire DecisionSite, USA and GraphPad Prism, USA). Ki values were calculated based on the Cheng-Prusoff equation, $K_i = IC_{50} / (1 + ([S]/K_m))$, with IC₅₀ values derived

from nonlinear curve fit of the dose response data using an outliers exclusion, variable slope model (Prism, Graphpad). Ki, inhibition constant; [S], substrate concentration; Km, Michaelis constant. Bidirectional hierarchical clustering was carried out on biochemical profiling data (Ki) for HDAC1–HDAC9 by creating a pairwise distance matrix using the unweighted pair group method with arithmetic mean and a Euclidean distance similarity measure (Spotfire DecisionSite, USA). Replicate experimental data from incubations with inhibitor were normalized to controls.

2.1.3. Chemo sensitivity assay

The effect of the new compounds on the proliferation of MCF7 and A549 cells was studied using the SulphoRhodamine-B (SRB) assay as previously described¹⁸. Doxorubicin and SAHA (Sigma, USA) were used as positive controls. Cells were seeded in a 96-well plate at a density of 10⁴ cells per well. After overnight incubation, cells were treated with HDAC inhibitors, doxorubicin or vorinostat (SAHA) (0.001–10 μmol L⁻¹), DMSO was added to the control cells and each treatment was performed in triplicate. After 48 h, cells were fixed and washed several times with water, and then stained with 0.4% SRB for 30 min and washed several times with 1% acetic acid solution. The retained dye was dissolved in 10 mM Tris base (pH 10.5) and color intensity was measured at 564 nm using an ELISA microplate reader (Thermo Scientific, USA). IC₅₀ values were calculated using the sigmoidal concentration–response curve-fitting model (Graph Pad, Prism software).

2.1.4. Measurement of caspase activity¹⁷

Effect of the new compounds and the positive control vorinostat (SAHA) on caspase7 activity was studied in MCF7 cells using the Caspase-glo 3/7 assay kit purchased from Promega (Madison, USA). The assay was carried out according to the manufacturer's procedure. In brief, exponentially growing 50% confluent cells were treated with the new compounds or the positive control vorinostat (1 and 3 μM). After 48 h, cells were collected and cell density was adjusted to 10⁶ cells/ml. The cell pellet was re-suspended in cell lysis buffer and the supernatant was collected by centrifugation at 4 °C. The cell extract was used to measure caspase activity by mixing in a 96-multiwell plate with a substrate. To calculate caspase activity, the absorbance was measured at 405 nm in an ELISA microplate reader (Meter tech. 960, USA).

2.1.5. Western blot

Effect of the new compounds on protein expression was measured by Western blot as previously described¹⁹. Exponentially growing, 50% confluent MCF7 cells were treated with 1 or 3 μM of the new HDAC inhibitors or vorinostat for 48 h. Control cells were treated with DMSO. Adherent cells were lysed using lysis buffer (1 mM Tris-HCl [pH 6.8], 2% w/v SDS, 10% glycerol, 2 mM PMSF), and a commercial protease inhibitor mixture (Complete Protease Inhibitor Mixture; Roche Molecular Biochemicals, Germany). Lysates were sonicated on ice, and the protein concentration was measured using a Bicinchoninic Acid (BCA) protein assay kit (Pierce-Life Technology, USA). A 30 μg fraction of the total cell lysate was loaded, resolved on SDS PAGE and electrotransferred to nitrocellulose membranes. Membranes were blocked using TBS-Tween 20 buffer containing 5% nonfat dried milk. The primary antibody solutions (1:1000; all Cell Signaling Technology) in 5% BSA TBS-T were incubated at 4 °C for overnight. Anti-species secondary antibody (Cell Signaling Technology) binding was carried out at room temperature for 1 h. Membranes were then washed three times for 10 min with TBS-T. Chemiluminescence detection was performed with an ECL plus Detection System (Pierce-Life Technology, USA). Quantification of the relative intensity of individual bands was carried out using the ChemiDoc Touch Imaging system from BioRad (USA) and band intensities were normalized to corresponding GAPDH level. Bands of untreated cells were used as a reference standard and intensities of other bands were expressed relative to them.

2.1.6. Cell cycle distribution analysis

Cell cycle studies were carried out using flow cytometry as described before²⁰. 5×10^5 cells were treated with 1 μ M of new HDAC inhibitor or vironostat. Control cells were treated with DMSO and incubated at 37 °C. Cells were collected at different time intervals (4, 24, 48 and 72 h), fixed in 70% ethanol, treated with RNase and then 50 μ L propidium iodide solution (1 mg/ml) was added and the DNA content was analyzed by flow cytometry using a FACS machine (Becton Dickenson, Germany).

2.1.7. RNA isolation

MCF7 cells were cultured in 175 cm² tissue culture flasks. After overnight incubation, exponentially growing 50% confluent cells were treated with 3 μ M of the compounds under investigation (**14**, **15**, **19**, **22** and **28** and vorinostat) for 24 h. At the end of the treatment period, cells were collected by centrifugation for 5 min at 300g and cell count was adjusted to 5×10^6 cells/ml. Total RNA was extracted using the ReliaPrep™ RNA cell miniprep system (Promega, USA) as described by the manufacturer. The RNA was quantified using Nanodrop. Studies were repeated in triplicate.

2.1.8. Whole transcriptome analysis

The RNA from MCF7 cells treated with compounds **14**, **15**, **19**, **22** and **28** and vorinostat for 24 h as well as a control of untreated MCF7 cells were treated with Turbo DNase (ThermoFisher, USA) and a whole transcriptome library was constructed using the Ion Ampliseq transcriptome kit targeting 21,000 genes. The library was enriched using the Ion OneTouch system (ThermoFisher, USA) and subject to Next Generation sequencing using the Ion Proton (ThermoFisher, USA) as described previously²¹.

2.1.9. Bioinformatics analysis

FASTQ files were converted to BAM files by aligning the genes to reference sequence HG19. The RNA count was carried out using the RPKM method to provide raw expression values of the genes. These were processed using the R script. The R script normalized the triplicate data using a negative binomial algorithm and the processed expression data was used to calculate the fold-change of genes related to HDAC enzymes, acetylated histones, survival, apoptosis and cell cycle markers. The fold-change was calculated by comparing each compound to the untreated control using vorinostat as the gold standard HDAC inhibitor as described previously²¹.

2.1.10. Procedure for the assessment of maximum kinetic aqueous solubility of **28**^{7,21}

Solubility assays were performed using Millipore MultiScreen® HTS-PFC Filter Plates designed for solubility assays (EMD Millipore, Billerica, MA, USA). The 96-well plates consist of two chambers separated by a filter. Liquid handling was performed using Janus® Verispan nd MTD workstations (Perkin Elmer, Waltham, MA, USA). Four microliters of drug solutions (10 mM in DMSO) are added to 196 μ L of phosphate-buffered saline (45 mM potassium phosphate, 45 mM sodium acetate, 45 mM ethanolamine, pH = 7.4) in the top chamber to give a final DMSO concentration of 2% and a theoretical drug concentration of 200 μ M. Plates are gently shaken for 90 min and then subjected to vacuum. Insoluble drug is captured on the filter. One hundred sixty microliters of the filtrate is transferred to 96-well Griener UV Star® analysis plates (Sigma-Aldrich, St. Louis, MO, USA) containing 40 μ L of acetonitrile. The drug concentration is measured by UV absorbance on a Spectromax® Plus microplate reader (Molecular Devices, Sunnyvale, CA, USA) using softmax Pro software v. 5.4.5 Absorbances at 5 wavelengths (280, 300, 320, 340 and 360 nm) were summed to generate the UV signal. Assays were performed in triplicate. Standard curves were generated by adding 4 μ L of 50x of five concentrations of **28** in DMSO to 40 μ L of acetonitrile in UV Star® plates followed by 156 μ L of phosphate buffered saline. Analysis and statistics were performed using GraphPad® Prism v. 5.04. Data are reported as the maximum concentration

observed in the filtrate.

2.1.11. Procedure for the assessment of mouse and human liver microsomal stability for **28**^{7,20,21}

The clearance of **28** in mouse or human liver microsomes was determined at 37 °C. Assays were conducted in 96-deep well polypropylene plates. Test compounds (1 μ M) were incubated in 0.5 mL of 100 mM potassium phosphate buffer (pH 7.4) with 0.5 mg/mL pooled liver microsomes from CD-1 mice (Life Technologies, Grand Island, NY, USA) or pooled liver microsomes from humans (ThermoFisher, Waltham, MA, USA), 2 mM tetra-sodium NADPH and 3 mM magnesium chloride for 60 min at 37 °C with gentle shaking. At five time points, 75 μ L of reaction mixture was transferred to 96-well shallow well stop plates on ice containing 225 μ L of acetonitrile with 0.1 mM propafenone as internal standard. Control reactions (lacking NADPH) were performed in a similar manner to demonstrate NADPH dependency of compound loss. Standard curves for **28** were generated using five concentrations in triplicate that were processed as above but with zero incubation time. Stop plates were centrifuged at 2000g for 10 min and then 170 μ L of the supernatants were transferred to a Waters Acquity® UPLC 700 μ L 96-well sample plate with cap mat (Waters, Milford, MA, USA). The amount of compound remaining in the supernatant was quantified by LC/MS/MS using a Waters TQ MS (electrospray positive mode) coupled to a Waters Acquity® UPLC (BEH column, C18, 1.7 μ m, 2.1 \times 50 cm, gradient of acetonitrile/water/0.1% formic acid). Propafenone was used as the internal standard. GraphPad® Prism v. 5.04 was used for nonlinear fitting of time course data to generate $t_{1/2}$ values. Results for assays lacking NADPH were expressed as percent of compound remaining after 69 min.

2.1.12. Procedure for the assessment of inhibitory activity of **28** for human CYP450 3A4^{7,20,21}

Inhibition of CYP3A4 was assessed by measuring the ability of **28** to inhibit the conversion of midazolam to 10-hydroxymidazolam. Ten concentrations of **28** were examined in triplicate (half-log serial dilutions). Assays were conducted in 1 mL 96-well polypropylene plates containing 100 μ L of 100 mM potassium phosphate buffer (pH 7.4), 3 mM magnesium chloride, 2 μ M midazolam, 1 mM tetra-sodium NADPH, Insect supersomes (Corning Gentest, Glendale, AZ, USA, containing 3 pmol/mL human CYP3A4, 47 nmol/min human P450 reductase activity, 14 pmol human cytochrome b5) and insect control microsome protein (Corning Gentest, Glendale, AZ, USA, 0.15 mg/mL). All components except NADPH were added to a prewarmed plate (37 °C) and reactions were initiated by adding NADPH. After 30 min, reactions were terminated with 200 μ L of acetonitrile containing 30 μ M prednisone as an internal standard. After centrifugation for 10 min at 2200g, 165 μ L of supernatants were transferred to an analysis plate. Samples were analyzed for 10-hydroxymidazolam concentration by LCMSMS as described above. IC50 values were determined using GraphPad® Prism v. 5.04 nonlinear curve fitting. The CYP3A4 inhibitor ketoconazole was used as a positive control.

2.1.13. Procedure for the assessment of inhibitory activity of **28** for human CYP450 2D6

Inhibition of CYP3A4 was assessed by measuring the ability of **28** to inhibit the conversion of AMMC (3-(2-(N,N-diethyl-N-methylammonium)ethyl)-7-methoxy-4-methylcoumarin) to AHMC (3-[2-(diethylaminoethyl)-7-hydroxy-4-methylcoumarin). Five concentrations of **28** were examined in triplicate (half-log serial dilutions). Assays were conducted in black 96-well 350 μ L polypropylene plates containing 100 μ L of 100 mM potassium phosphate buffer (pH 7.4), 3 mM magnesium chloride, 1 μ M AMMC, 0.1 mM tetra-sodium NADPH, insect supersomes (Corning Gentest, Glendale, AZ, USA, containing 4 pmol/mL human CYP2D6 and 100 nmol/min human P450 reductase activity), and insect control microsome protein (Corning Gentest, Glendale, AZ, USA, 0.15 mg/mL). All components except NADPH were added to a

prewarmed plate (37 °C) and reactions were initiated by adding NADPH. After 40 min reactions were terminated with 75 μ L of 0.5 M Tris base:acetonitrile (1:4). Samples were analyzed for AMHC concentration by reading fluorescent intensity at 470 nm (excitation at 405 nm) in an Envision plate reader (Perkin Elmer, Waltham, MA, USA). Fluorescent intensity was corrected for test compound fluorescence. IC₅₀ values were determined using GraphPad® Prism v. 5.04 nonlinear curve fitting. The CYP2D6 inhibitor quinidine was used as a positive control.

2.1.14. Procedure for the assessment of inhibitory activity of **28** for human CYP450 2C9

Inhibition of CYP2C9 activity was assessed by measuring the ability of **28** to inhibit conversion of MFC (7-methoxy-4-(trifluoromethyl)-coumarin) to HFC (7-hydroxy-4-(trifluoromethyl)-coumarin). Five concentrations of **28** were examined in triplicate (half-log serial dilutions). Assays were conducted in black 96-well polypropylene plates containing 100 μ L of 100 mM Tris-HCl (pH 7.4), 3 mM magnesium chloride, 70 μ M MMC, 1 mM tetra-sodium NADPH, insect supersomes (Corning Gentest, Glendale, AZ, USA, containing 25 pmol/mL human CYP2C9-1(Arg₁₄₄) and 70 nmol/minute human P450 reductase activity), and insect control microsome protein (Corning Gentest, Glendale, AZ, USA, 0.15 mg/mL). All components except NADPH were added to a prewarmed plate (37 °C) and reactions were initiated by adding NADPH. After 30 min reactions were terminated with 75 μ L of 0.5 M Tris base:acetonitrile (1:4). Samples were analyzed for HFC concentration by reading fluorescent intensity at 530 nm (excitation at 430 nm) in an Envision plate reader (Perkin Elmer, Waltham, MA, USA). Fluorescent intensity was corrected for test compound fluorescence. IC₅₀ values were determined using GraphPad® Prism v. 5.04 nonlinear curve fitting. The CYP2C9 inhibitor sulfaphenazole was used as a positive control.

2.1.15. Statistical analysis

Data are represented as mean \pm SEM and analyzed statistically by ANOVA using Graphpad Prism software (GraphPad Software, USA). The comparison of the effect of the compounds on the HDAC classes was carried out using Anova followed by Bonferroni post hoc analysis. The statistical significance between groups was defined as * p < 0.05, ** p < 0.01 and *** p < 0.001.

2.2. Chemistry

2.2.1. General methods⁵¹

Chemical reagents and anhydrous solvents were purchased from Sigma-Aldrich (USA) and were used without further purification. Solvents for extraction and column chromatography were distilled prior to use. TLC analysis was performed with silica gel plates (0.25 mm, E. Merck, 60 F₂₅₄) using iodine and a UV lamp for visualization. Retention factor (R_f) values were measured using a 5 \times 2 cm TLC plate in a developing chamber containing the solvent system described. Melting points were measured with a Stuart Melting Point Apparatus (SMP30) in Celsius degrees and were uncorrected. ¹H, ¹³C NMR and 2D-NMR experiments were performed on a 500 MHz instrument. Chemical shifts are reported in parts per million (ppm) downstream from the internal tetramethylsilane standard. Spin multiplicities are described as s (singlet), d (doublet), dd (double doublets), t (triplet), (td) triple doublets or m (multiplet). Coupling constants are reported in Hertz (Hz). ESI mass spectrometry was performed on a Q-TOF high-resolution mass spectrometer or Q-TOF UltiM LC-MS. Optical rotations were measured with a digital polarimeter using a 100 mm cell of 10 mL capacity. Single-crystal X-ray diffraction data were collected using an Oxford Diffraction XCalibur, equipped with (Mo) X-ray Source (λ = 0.71073 Å) at 293(2) K. HPLC purification was performed on an Agilent 1260 infinity series HPLC spectrometer, using a Restek Ultra AQ C18 5 μ m 150 mm \times 4.6 mm column, eluted using 0.1% TFA in water and acetonitrile at 1.0 mL/min and detected at 220 nm. Compound purity was assured by a combination of high-field multinuclear NMR (¹H, ¹³C), HRMS (ESI-TOF) and

HPLC; purity by the later was always > 95%. The synthesis of the tested compounds is described in the [supplementary material](#) (Figs. S1–S15). All compounds (**14**, **15**, **19**, **22**, and **28**) were dissolved in 100% DMSO (Sigma Aldrich, USA) and were diluted in medium just before use. The maximum concentration of DMSO did not exceed 0.5% in all experiments and DMSO was utilized as a negative control. Vorinostat (SAHA, Sigma Aldrich, USA) and MAZ1914 were used as positive controls.

2.2.2. Molecular modeling

The X-ray crystal structures of HDAC1 (PDB: 6Z2J²²), HDAC2 (PDB: 6WBZ²³), HDAC3 (PDB: 4A69²⁴), HDAC4 (PDB: 6FYZ²⁵), HDAC6 (PDB: 5EDU²⁶) and HDAC7 (PDB: 3C0Z²⁷) were downloaded from the RCSB Protein Data Bank (www.rcsb.org). Homology models were prepared for HDAC5 and HDAC9. The amino acid sequences of the histone deacetylase domain were retrieved from uniprot database (HDAC5: Q9UQL6 | 684-1028 and HDAC9: Q9UKV0 | 631-978, www.uniprot.org). Blast homology search engine²⁸ was used to search for sequence homologs. The crystal structure of the catalytic domain of HDAC4 in complex with a hydroxamic acid inhibitor (PDB: 2VQM²⁹) was used as template for both HDAC5 and HDAC9. The template has a percent identity of 77% with HDAC5 and 73% with HDAC9, which ensures high reliability models. The models were built and validated using Prime³⁰⁻³². All protein structural files were prepared to adjust bond orders, add missing hydrogen, complete missing side chains and amino acid residues. Water molecules were deleted. The hydrogen bond network was optimized, and the structure was then relaxed. Protein preparation was performed by RprepWizard³³⁻³⁴. The atomic coordinates of the hydroxamic acid inhibitor were copied from HDAC4 to all targets and the protein–ligand complexes were then thoroughly minimized. The ligand was selected to define the receptor grid. Ligands were prepared in LigPrep³⁵. Soft docking approach in Glide³⁶⁻³⁹ was used to find the best binding mode of each compound.

2.2.3. General reaction procedure for the preparation of 3-(3-(tert-butylamino)imidazo[1,2-a]pyridin-2-yl)benzoic acid (**5**) and 3-(3-(tert-butylamino)imidazo[1,2-a]pyridin-2-yl)benzoic acid (**6**)⁴⁰

Scandium triflate (20 mol%) and sodium sulfate (2.0 mmol) were added to a solution of aldehyde (**1**, 1.0 mmol) and 2-aminoazine (**2/3**, 1.0 mmol) in MeOH:DCM (3:1 mL) at rt. After 45 min, *tert*-butyl isocyanide (**4**, 1.1 mmol) was introduced and stirring was continued at rt for 12–15 h. After completion, MeOH and DCM were removed. The residue was diluted with DCM (100 mL) and washed with water (3 \times 50 mL). Then, the organic layer was dried over Na₂SO₄ and concentrated under vacuum. The crude product was purified on flash chromatography using 80% EtOAc in hexane as eluent to produce compound **5/6** as white solid.

2.2.4. General reaction procedure for the preparation of *N*-(2-amino-5-cyanophenyl)-3-(3-(tert-butylamino)imidazo[1,2-a]pyridin-2-yl)benzamide (**8**) and *N*-(2-amino-5-cyanophenyl)-3-(3-(tert-butylamino)imidazo[1,2-a]pyridin-2-yl)benzamide (**9**)⁴⁰

Compound **5/6** (1.0 mmol) and DIPEA (1.4 mmol) were mixed in anhydrous DMF (8 mL) at 0 °C. After 45 min, HBTU (1.2 mmol), followed by the amine partner (**7**; 1.0 mmol), were added and stirring was continued at rt for 10–13 h. After completion, the reaction mixture was diluted with EtOAc (50 mL) and washed with cold water (3 \times 30 mL) and brine solution (10 mL). Then, the organic layer was dried over Na₂SO₄ and concentrated under vacuum. The crude product was purified on flash chromatography using EtOAc/hexane as eluent to obtain the title compound **8/9**. The obtained regioisomeric mixture was used directly in the next step without any further purification.

2.2.5. General reaction procedure for the preparation of 2-(3-(3-(tert-butylamino)imidazo[1,2-a]pyridine-2-yl)phenyl)-1H-benzo[d]imidazole-5-carbonitrile (**10**) and 2-(3-(3-(tert-butylamino)imidazo[1,2-a]pyridin-2-yl)phenyl)-1H-benzo[d]imidazole-5-carbonitrile (**11**)⁴⁰

Compound (**8/9**), 0.5 mmol) was dissolved in acetic acid (3 mL) and refluxed for 24 h. After completion, acetic acid was removed and the crude product was recrystallized from EtOAc to give compounds **10/11**.

2.2.6. General reaction procedure for the preparation of 2-(3-(3-(tert-butylamino)imidazo[1,2-a]pyridine-2-yl)phenyl)-N-hydroxy-1H-benzo[d]imidazole-5-carboximidamide (**12**) and 2-(3-(3-(tert-butylamino)imidazo[1,2-a]pyridin-2-yl)phenyl)-N-hydroxy-1H-benzo[d]imidazole-5-carboximidamide (**13**)

A mixture of Na₂CO₃ (0.25 mmol), NH₂OH.HCl (0.25 mmol) and compound **10/11** in ethanol (1.5 mL) was heated under reflux for 24 h. After completion, the EtOH was removed. The residue was diluted with EtOAc (20 mL) and washed with water (3 × 10 mL). Then, the organic layer was dried over Na₂SO₄ and concentrated under vacuum to produce compound **12/13** as a white solid.

2.2.7. 2-(3-(3-(tert-butylamino)imidazo[1,2-a]pyridine-2-yl)phenyl)-N-hydroxy-1H-benzo[d]imidazole-5-carboximidamide (**12**)

Brownish solid. 136 mg, 62% yield. mp 226–228 °C. ¹H NMR (500 MHz, DMSO) δ 9.57 (s, 1H), 8.96 (s, 1H), 8.45 (d, *J* = 6.9 Hz, 1H), 8.34 (d, *J* = 7.8 Hz, 1H), 8.11 (d, *J* = 7.8 Hz, 1H), 7.90 (s, 1H), 7.58 (t, *J* = 7.7 Hz, 3H), 7.51 (d, *J* = 9.0 Hz, 1H), 7.26–7.18 (m, 1H), 6.91 (t, *J* = 6.7 Hz, 1H), 5.83 (s, 2H), 4.74 (s, 1H), 1.03 (s, 8H). ¹³C NMR (125 MHz, DMSO) δ 168.5, 152.4, 151.6, 141.2, 137.4, 136.1, 129.9, 129.1, 128.5, 127.5, 125.8, 125.0, 124.4, 124.3, 124.2, 120.1, 116.7, 111.2, 55.9, 30.08. LCMS (ESI): *m/z* 440 [M + H]⁺.

2.2.8. General reaction procedure for the preparation of compounds **14/15**

A mixture of trifluoroacetic anhydride (0.3 mmol) and compound **12/13** (0.25 mmol) in pyridine (1 mL) was heated under reflux for 3 h. After completion, reaction mixture was concentrated. The residue was diluted with EtOAc (50 mL) and washed with solution of NaHCO₃ (3 × 20 mL). The organic layer was dried over Na₂SO₄ and concentrated under vacuum. The crude product was purified on flash chromatography to produce compound **14/15** as white solid.

2.2.9. N-(Tert-butyl)-2-(3-(5-(5-(trifluoromethyl)-1,2,4-oxadiazol-3-yl)-1H-benzo[d]imidazol-2-yl)phenyl)imidazo[1,2-a]pyridine-3-amine (**14**)

White solid. 58 mg, 45% yield. mp 135–137 °C. ¹H NMR (500 MHz, CD₃OD) δ 8.92 (d, *J* = 6.1 Hz, 1H), 8.75 (s, 1H), 8.42 (s, 1H), 8.27 (d, *J* = 7.4 Hz, 1H), 8.16–8.05 (m, 2H), 8.00 (t, *J* = 7.9 Hz, 1H), 7.91 (d, *J* = 8.7 Hz, 1H), 7.83 (t, *J* = 7.8 Hz, 2H), 7.55 (t, *J* = 6.7 Hz, 1H), 1.10 (s, 9H). ¹³C NMR (125 MHz, CD₃OD) δ 169.6, 165.5, 153.2, 141.3, 139.2, 137.7, 133.5, 130.4, 129.9, 129.8, 129.6, 129.1, 127.7, 126.3, 125.9, 122.3, 119.8, 116.5, 116.2 (q, 1JC-F = 271.2 Hz), 115.5, 114.9, 111.7, 56.3, 29.0. HRMS (ESI-TOF): *m/z* calcd for C₂₇H₂₃F₃N₇O 518.1916, found 518.1904 [M + H]⁺.

2.2.10. N-(Tert-butyl)-2-(3-(5-(5-(trifluoromethyl)-1,2,4-oxadiazol-3-yl)-1H-benzo[d]imidazol-2-yl)phenyl)imidazo[1,2-a]pyridin-3-amine (**15**)

White solid. 62 mg, 48% yield. mp 164–166 °C. ¹H NMR (500 MHz, CD₃OD) δ 8.93 (d, *J* = 1.4 Hz, 1H), 8.79 (t, *J* = 1.5 Hz, 1H), 8.49 (dd, *J* = 4.7, 1.4 Hz, 1H), 8.46–8.27 (m, 1H), 8.25–8.19 (m, 1H), 8.17–8.13 (m, 1H), 8.05 (dd, *J* = 8.5, 1.5 Hz, 1H), 7.92 (d, *J* = 4.7 Hz, 1H), 7.89–7.73 (m, 1H), 7.70 (t, *J* = 7.8 Hz, 1H), 1.07 (s, 9H). ¹³C NMR (125 MHz, CD₃OD) δ 171.0, 166.6, 155.3, 143.3, 142.4, 138.4, 138.3, 136.3, 132.1, 131.9, 130.5, 130.4, 130.2, 129.7, 128.2, 128.0, 127.7, 127.6, 123.3, 120.7, 117.6 (q, 1JC-F = 271.2 Hz), 114.3, 57.7, 30.5. HRMS (ESI-TOF): *m/z* calcd for C₂₆H₂₂F₃N₈O 519.1868, found 519.1854 [M + H]⁺.

2.2.11. Procedure for the preparation of 4-(3-(tert-butylamino)imidazo[1,2-a]pyridine-2-yl)benzotrile (**17**)⁴¹

Scandium triflate (20 mol%) and sodium sulfate (2.0 mmol) were added to a solution of aldehyde (**16**, 1 mmol) and 2-aminopyridine (**3**, 1 mmol) in MeOH:DCM (3:1 mL) at rt. After 45 min, *tert*-butyl isocyanide (**4**, 1.1 mmol) was introduced and stirring was continued at rt for 12–15 h. After completion, MeOH and DCM were removed under vacuum. The residue was diluted with DCM (100 mL) and washed with water (3 × 50 mL). The organic layer was dried over Na₂SO₄ and concentrated under vacuum. The crude product was purified on flash chromatography using 40% EtOAc in hexane as eluent to produce compound **17** as white solid. 429 mg, 74% yield.

2.2.12. Procedure for the preparation of 4-(3-(tert-butylamino)imidazo[1,2-a]pyridine-2-yl)-N-hydroxybenzimidamide (**18**)

A mixture of Na₂CO₃ (0.5 mmol), NH₂OH.HCl (0.5 mmol) and compound **17** (0.1 mmol) in ethanol (2 mL) was heated under reflux for 24 h. After completion, the EtOH was removed. The residue was diluted with EtOAc (30 mL) and washed with water (3 × 10 mL). The organic layer was dried over Na₂SO₄ and concentrated under vacuum to produce compound **12** as white solid. 24 mg, 74% yield. mp 238–240 °C. ¹H NMR (500 MHz, CD₃OD) δ 8.44 (d, *J* = 6.9 Hz, 1H), 8.07 (d, *J* = 8.4 Hz, 2H), 7.75 (d, *J* = 8.4 Hz, 2H), 7.49 (d, *J* = 9.0 Hz, 1H), 7.33–7.27 (m, 1H), 6.95 (t, *J* = 6.8 Hz, 1H), 1.04 (s, 9H). ¹³C NMR (125 MHz, CD₃OD) δ 162.1, 155.4, 155.4, 143.4, 139.3, 137.7, 129.4, 127.1, 126.5, 125.4, 117.1, 113.0, 57.0, 30.6. LCMS (ESI): *m/z* 324 [M + H]⁺.

2.2.13. Procedure for the preparation of N-(tert-butyl)-2-(4-(5-(trifluoromethyl)-1,2,4-oxadiazol-3-yl)phenyl)imidazo[1,2-a]pyridine-3-amine (**19**)

A mixture of trifluoroacetic anhydride (0.3 mmol) and compound **18** (0.25 mmol) in pyridine (1 mL) was heated under reflux for 3 h. After completion, reaction mixture was concentrated. The residue was diluted with EtOAc (50 mL) and washed with solution of NaHCO₃ (3 × 20 mL). The organic layer was dried over Na₂SO₄ and concentrated under vacuum. The crude product was purified on flash chromatography to produce **19** as white solid. 55 mg, 55% yield. mp 178–180 °C. ¹H NMR (500 MHz, CD₃OD) δ 8.39 (dd, *J* = 6.9, 0.9 Hz, 1H), 8.25–8.16 (m, 4H), 7.50 (d, *J* = 9.0 Hz, 1H), 7.30–7.25 (m, 1H), 6.95–6.87 (m, 1H), 1.05 (s, 9H). ¹³C NMR (125 MHz, CD₃OD) δ 169.0, 165.6, 142.2, 139.0, 137.2, 128.7, 127.4, 125.4, 125.1, 123.9, 123.6, 116.2, 116.1 (q, 1JC-F = 273.4 Hz), 111.9, 56.0, 29.7. HRMS (ESI-TOF): *m/z* calcd for C₂₀H₁₉F₃N₅O 402.1541, found 402.1530 [M + H]⁺.

2.2.14. Procedure for the preparation of 3-(3-(tert-butylamino)imidazo[1,2-a]pyridine-2-yl)benzoic acid (**20**)⁴⁰

Scandium triflate (20 mol%) and sodium sulfate (2.0 mmol) were added to a solution of aldehyde (**1**, 1.0 mmol) and 2-aminoazine (**2**, 1.0 mmol) in MeOH:DCM (3:1 mL) at rt. After 45 min, *tert*-butyl isocyanide (**4**, 1.1 mmol) was introduced and stirring was continued at rt for 12–15 h. After completion, MeOH and DCM were removed. The residue was diluted with DCM (100 mL) and washed with water (3 × 50 mL). Then, the organic layer was dried over Na₂SO₄ and concentrated under vacuum. The crude product was purified on flash chromatography using 80% EtOAc in hexane as eluent to produce compound **20** as white solid. 241 mg, 78% yield.

2.2.15. Procedure for the preparation of N-(2-amino-4-fluorophenyl)-3-(3-(tert-butylamino)imidazo[1,2-a]pyridine-2-yl)benzamide (**22**)^{13,51}

Compound **20** (0.5 mmol) and DIPEA (0.7 mmol) were mixed in anhydrous DMF (4 mL) at 0 °C. After 45 min, HBTU (0.6 mmol) and amine (**21**, 0.5 mmol) were added and stirring was continued at rt for 10–13 h. After completion, the reaction mixture was diluted with EtOAc (50 mL), washed with cold water (3 × 30 mL) and brine solution (10 mL). The organic layer was dried over Na₂SO₄ and concentrated under vacuum. The crude product was purified on flash chromatography using

EtOAc/hexane as eluent to produce **22** as white solid. 145 mg, 70% yield. mp 299–301 °C. ¹H NMR (500 MHz, CD₃OD) δ 8.52 (s, 1H), 8.40 (d, *J* = 6.9 Hz, 1H), 8.17 (d, *J* = 7.8 Hz, 1H), 7.96 (d, *J* = 7.8 Hz, 1H), 7.59 (t, *J* = 7.8 Hz, 1H), 7.50 (d, *J* = 9.0 Hz, 1H), 7.33–7.27 (m, 1H), 7.20 (dd, *J* = 8.6, 5.9 Hz, 1H), 6.93 (t, *J* = 6.8 Hz, 1H), 6.61 (dd, *J* = 10.5, 2.7 Hz, 1H), 6.47 (d, *J* = 2.7 Hz, 1H), 1.04 (s, 9H). ¹³C NMR (125 MHz, CD₃OD) δ 167.6, 162.2 (d, 1J_{C-F} = 268.4 Hz), 144.4, 141.8, 137.4, 134.9, 134.0, 131.6, 128.6, 128.0, 127.2, 126.8, 125.7, 124.6, 124.0, 119.3, 115.9, 112.1, 104.6, 103.2, 56.0, 29.8. HRMS (ESI-TOF): *m/z* calcd for C₂₄H₂₅FN₅O 418.2043, found 418.2033 [M + H]⁺.

2.2.16. Procedure for the preparation of 3-(imidazo[1,2-*a*]pyridine-2-yl)benzonitrile (**24**)⁴²

A mixture of compound **23** (3 mmol) and **2** (2.7 mmol) in ethanol (12 mL) was heated under reflux. After 3 h, the reaction mixture was cooled and NaHCO₃ was added at rt. After 30 min, the reaction mixture was heated at 80 °C for 12 h. After completion, EtOH was removed under vacuum. The crude was diluted with DCM (100 mL) and washed with water (3 × 50 mL). Then, the organic layer was dried over Na₂SO₄ and concentrated under vacuum. The crude product was recrystallized using a mixture of EtOAc and hexane to produce compound **16** as white solid. 446 mg, 68% yield.

2.2.17. 2.2.18. Procedure for the preparation of 3-(imidazo[1,2-*a*]pyridine-2-yl)benzoic acid (**25**)⁴⁰

A mixture of compound **23** (2 mmol) and 6 N NaOH (6.3 mL) was heated under reflux for 3 h. After completion, EtOH was removed under vacuum. The residue was diluted with water (100 mL) and acidified with 1 M HCl until it forms a precipitate. The precipitate was isolated by filtration and dried to obtain compound **17** as white solid. 290 mg, 61% yield.

2.2.18. Procedure for the preparation of *N*-(2-amino-4-cyanophenyl)-3-(imidazo[1,2-*a*]pyridine-2-yl)benzamide (**26**)⁴⁰

Compound **24** (1.0 mmol) and DIPEA (1.4 mmol) were mixed in anhydrous DMF (8 mL) at 0 °C. After 45 min, HBTU (1.2 mmol), followed by the amine partner (7; 0.1 mmol), were added and stirring was continued at room temperature for 10–13 h. After completion, the reaction mixture was diluted with EtOAc (50 mL) and washed with cold water (3 × 30 mL) and brine solution (10 mL). Then, the organic layer was dried over Na₂SO₄ and concentrated under the vacuum to obtain the crude product, which was purified on flash chromatography using EtOAc/hexane as eluent to obtain the title compound **26**. The obtained regioisomeric mixture was used directly in the next step without any further purification. 264 mg, 75% yield.

2.2.19. Procedure for the preparation of 2-(3-(imidazo[1,2-*a*]pyridine-2-yl)phenyl)-1*H*-benzo[*d*]imidazole-6-carbonitrile (**27**)⁴⁰

A solution of compound **26** (0.5 mmol) in acetic acid (3 mL) was refluxed for 24 h. After completion, acetic acid was completely removed and crude product was recrystallized in EtOAc to obtain compound **27** as brownish solid. 119 mg, 71% yield.

2.2.20. Procedure for the preparation of *N*-hydroxy-2-(3-(imidazo[1,2-*a*]pyridine-2-yl)phenyl)-1*H*-benzo[*d*]imidazole-6-carboximidamide (**28**)

A mixture of trifluoroacetic anhydride (0.3 mmol) and compound **27** (0.25 mmol) in pyridine (1 mL) was heated under reflux for 3 h. After completion, reaction mixture was dried. The residue was diluted with EtOAc (50 mL) and washed with solution of NaHCO₃ (3 × 20 mL). The organic layer was dried over Na₂SO₄ and concentrated under vacuum. The crude product was purified on flash chromatography to produce **27** as a brownish solid. 55 mg, 60% yield. mp 245–247 °C. ¹H NMR (500 MHz, CD₃OD) δ 8.50 (s, 1H), 8.30 (d, *J* = 6.7 Hz, 1H), 8.13 (s, 1H), 8.02–7.95 (m, 2H), 7.83 (s, 1H), 7.57–7.48 (m, 4H), 7.26–7.19 (m, 1H), 6.88–6.80 (m, 1H). ¹³C NMR (125 MHz, DMSO) δ 152.6, 152.1, 145.4, 144.3, 135.1, 131.1, 129.9, 128.1, 127.5, 127.4, 126.2, 125.7, 124.1,

120.6, 117.2, 112.9, 110.0. HRMS (ESI-TOF): *m/z* calcd for C₂₁H₁₇N₆O 369.1463, found 369.1455 [M + H]⁺.

3. Results

3.1. Chemistry

3.1.1. Novel inhibitors discovery

Recently, we reported the synthesis of a three series of imidazopyridine derivatives employing post-transformation of the Groebke-Blackburn-Bienaym *e* [4 + 1]-cycloaddition reaction products¹³. The ultimate goal of these efforts was to establish compound libraries of privileged scaffolds for our drug discovery campaign. Some of these derivatives showed promise as starting points for anticancer⁴³, antibacterial⁴⁴ and BACE1 inhibitor (one of the most important enzymes involved in Alzheimer's disease pathology), drug discovery⁴⁵. In continuation of these efforts, selected compounds from these libraries were examined in a screening campaign against various HDAC isoforms. This initiative was inspired by the variety of cap and metal-chelating groups present in various HDACs inhibitors. As a result, we identified novel chemotypes bearing the imidazopyridine core scaffold, as shown in Fig. 1B.

HDAC inhibitors, including vorinostat, share three common structural motifs: a zinc binding moiety (e.g., hydroxamic acid), a tether occupying the hydrophobic sub-pocket in the active site, and a functional cap group that resides outside the hydrophobic hollow and interacts with the HDAC exterior amino acid residues (Fig. 1B). HDAC inhibitors are known to accommodate a wide variety of metal-chelating groups, which allows for the replacement of this group with various bioisosters (e.g., the trifluoromethyl oxadiazole (TMFO) moiety),⁴⁶ while maintaining their activities and enhancing their selectivity toward certain HDAC isoforms. Our approach was to apply these characteristics to our newly discovered chemical scaffold and evaluate the binding topographies of various HDAC inhibitors.

We hypothesized that an isophthalic acid core substituted with an imidazopyridine group on one side and a substituted five-membered heterocyclic ring on the other side might deliver novel motifs that selectively inhibit HDACs. To this end, we tested *in vitro* an in-house collection of small molecules encompassing various skeletal and structural diversity including imidazopyridine core scaffold. The latter should represent the cap group and, together with the *meta*-disubstituted benzene core, should provide an optimal linker for incorporating a hydroxamic acid functionality or other metal- and/or non-metal-chelating groups such as the TMFO moiety, which has been reported to enhance the selectivity toward HDACs as a non-metal binding group (MBG)⁴⁶. Then, a concise set of heterocyclic scaffolds with an embedded imidazopyridine moiety was studied using docking protocols. The structures of these analogues possessed: (1) an imidazopyridine cap group; (2) an isophthalic acid core; (3) imidazole moieties, and (4) a hydroxamic acid or TFMO group to fit into the zinc binding pocket of HDACs either as a metal-chelating or a metal non-chelating group, respectively (Fig. 1B).

The decision to include an oxadiazole ring as an isosteric replacement for the hydroxamic acid appendage was based on earlier report indicating that this group enhances the selectivity toward HDACs⁴⁶. Additionally, an H-bond acceptor (e.g., CF₃-group) attached to this moiety might improve the selectivity and lead to strong interactions with the catalytic amino acid residues in the enzyme active site. Therefore, the phenyl ring portion of compound **I** was swapped with an imidazopyridine group to enhance affinity for HDACs, leading to compounds of type **II**, containing an imidazole-like linker connected to a non-zinc chelating binding motif like TFMO, and type **III**, containing the traditional hydroxamic acid zinc-chelating moiety. To reduce the flexibility present in vorinostat, the amide group was embedded into the rigid imidazopyridine moiety system, which retains the essential hydrogen bonding interactions with the amino acid residues in the active site and provided suitable vectors for direct extensions into the

corresponding sub-pockets of the active sites (Fig. 1B). Additional rigidity was obtained by replacing the flexible alkyl chain of vorinostat with a benzimidazole linker. We envisioned that these concepts should provide new classes of inhibitors with enhanced potency and selectivity. Our results are summarized in Table 1.

3.1.2. Synthesis

The preparation of the most promising compounds in this study was carried out as described in Schemes 1–4. Since our modeling studies predicted that the most potent compounds would fall within Classes II and III (Fig. 1B), we focused our synthetic efforts on those scaffolds. Four variations were synthesized. The first variant involved linking an imidazopyridine cap group to a zinc-chelating or metal none-chelating binding group through a linker containing a *meta*-substituted phenyl ring and a benzimidazole moiety (Scheme 1A). These disubstituted isophthalic acid scaffolds were assembled starting with isophthalaldehyde (1). This starting material was treated in a multicomponent [4 + 1]-cycloaddition reaction with either 2 or 3, followed by *tert*-butyl isocyanide (4), to deliver the Groebke-Blackburn-Bienaymé products 5 and 6, respectively, which were subsequently used without purification. These intermediates were then subjected to a coupling reaction with the phenylenediamine derivative 7, followed by acid catalyzed cyclization, to give the benzimidazole derivatives 10 and 11. Treatment of 10 and 11 with hydroxyl amine delivered the hydroxamic acids 12 and 13, respectively. Reaction of these two intermediates with trifluoroacetic anhydride delivered the desired trifluoro-oxadiazole derivatives, 14 and 15.

In the second variant (Scheme 1B), 4-cyanobenzaldehyde (16) was reacted with *tert*-butyl isocyanide (4) and 2-aminopyridine (2) to give the [4 + 1]-cycloaddition product 17. The latter was then reacted with hydroxyl amine to deliver the hydroxamic acid 18, which was treated with trifluoroacetic anhydride (TFAA) to furnish compound 19.

For the synthesis of the third class of compounds (Scheme 2A), compound 1 was reacted with *tert*-butyl isocyanide (4) and 2-aminopyridine (2) to deliver the [4 + 1]-cycloaddition product 20. Coupling of 20 with phenylenediamine 21 in the presence of 2-(1H-benzotriazole-1-yl)-1,1,3,3-tetramethylammonium tetrafluoroborate (TBTU) and diisopropylethylamine (DIPEA) gave compound 22. The region-isomeric structure of compound 22 is unambiguously confirmed by extensive 2D-NMR experiments, including HMBC and NOESY (See Scheme 2A and Supporting information).

For the synthesis of 28 (the fourth variant), the 3-cyano α -bromoketone 23 was reacted with 2-aminopyridine (2) using NaHCO₃ in refluxing EtOH to give compound 24 (Scheme 2B). Hydrolysis of 24 in the presence of alcoholic NaOH yielded intermediate 25, which was coupled with phenylenediamine 7 in the presence of TBTU and DIPEA to give compound 26. Intermediate 26 was subjected to cyclization through the amide carbonyl group by treatment with NH₄OAc in acetic acid followed by chromatographic purification on silica gel to deliver compound 27. This intermediate was finally reacted with hydroxyl amine to give the hydroxamic acid 28.

3.1.3. Identification of initial candidates by molecular modeling

To gain insight into the binding modes of the most potent motifs, we docked a representative set of heterocyclic scaffolds with an embedded imidazopyridine moiety anchored to a phthalic acid core to the crystal

structures of HDAC1–4, HDAC6 and HDAC7, and the homology models of HDAC5 and HDAC9.

HDAC isoforms are structurally similar, which imposes challenges in achieving target selectivity. Structure alignment revealed their close resemblance and in particular with regard to the active site (Fig. 2). The values of all-atoms root mean square deviation (RMSD) using HDAC1 as the frame of reference range from 1.297 Å for HDAC2 to 5.123 Å for HDAC5. Compound 28 was predicted to fit better in HDAC1 and HDAC2 (Fig. 3 and 4), with docking scores of –8.013 kcal/mol and –9.493 kcal/mol, respectively. The *N*-hydroxyformimidamide is in close proximity to the Zn⁺² ion (2.1 Å for HDAC1 and 2.3 Å for HDAC2), to which it coordinates through its nitrogen and oxygen atoms. Compound 28 forms strong hydrogen bond to His141 and electrostatic interactions with Glu98, Asp99, Asp174, Asp176, His179 and Lys200 in active site of HDAC1. For HDAC2, similar hydrogen bonds were observed with His179, Tyr304 and Gly150. Electrostatic interactions were detected with His29, Arg35, Asp175, Asp177, Asp182 and His180. These various interactions ensure proper orientation of 28 in the binding sites. In addition, 28 forms π - π contacts with Phe150 in HDAC1. The hydrophobic phenyl imidazopyridine group is located in the solvent exposed region of the binding sites of HDAC1 and HDAC2 and, as such, does not require the loss of significant amounts of desolvation energy, which may contribute to the high affinity of 28 towards both enzymes. Compound MAZ1914 was predicted to bind with less affinity to both targets in our models, giving docking scores of –5.074 kcal/mol for HDAC1 and –6.439 kcal/mol for HDAC2. The oxadiazole interacts in the same way as that of the hydroxylformimidamide group of 28.

In general, the compounds that show considerable activities against HDAC targets are those that can coordinate with Zn⁺² ion in the binding pockets. The compounds appear to orient the hydroxamate, oxadiazole, hydroxyformimidamide or similar group to interact with Zn⁺² and/or aspartate and histidine amino acids that coordinate Zn⁺² in the binding sites. The more active compounds also show additional interactions that augment ligand affinity including hydrogen bonding with side chain and backbone N/O atoms, π - π stacking with Phe/His residues, aromatic bonds with polar amino acids, cation- π interactions with Arg residues, and hydrophobic contacts with several amino acids in the binding pockets. Although some molecular fragments are solvent exposed, which can reduce the biological activity if the compounds have to go through an energetically unfavorable desolvation step, these fragments in most of the cases are hydrophobic in nature and should not suffer significantly from the loss in binding affinity.

3.2. In vitro drug-like properties

To investigate the drug-like properties of our new chemical scaffold we examined 28 in a battery of *in vitro* physicochemical/ADME assays. These assays are routinely used in drug discovery to assess the potential for metabolism and drug-drug interactions and predict *in vivo* exposure and bioavailability. Our results are presented in Table 1.

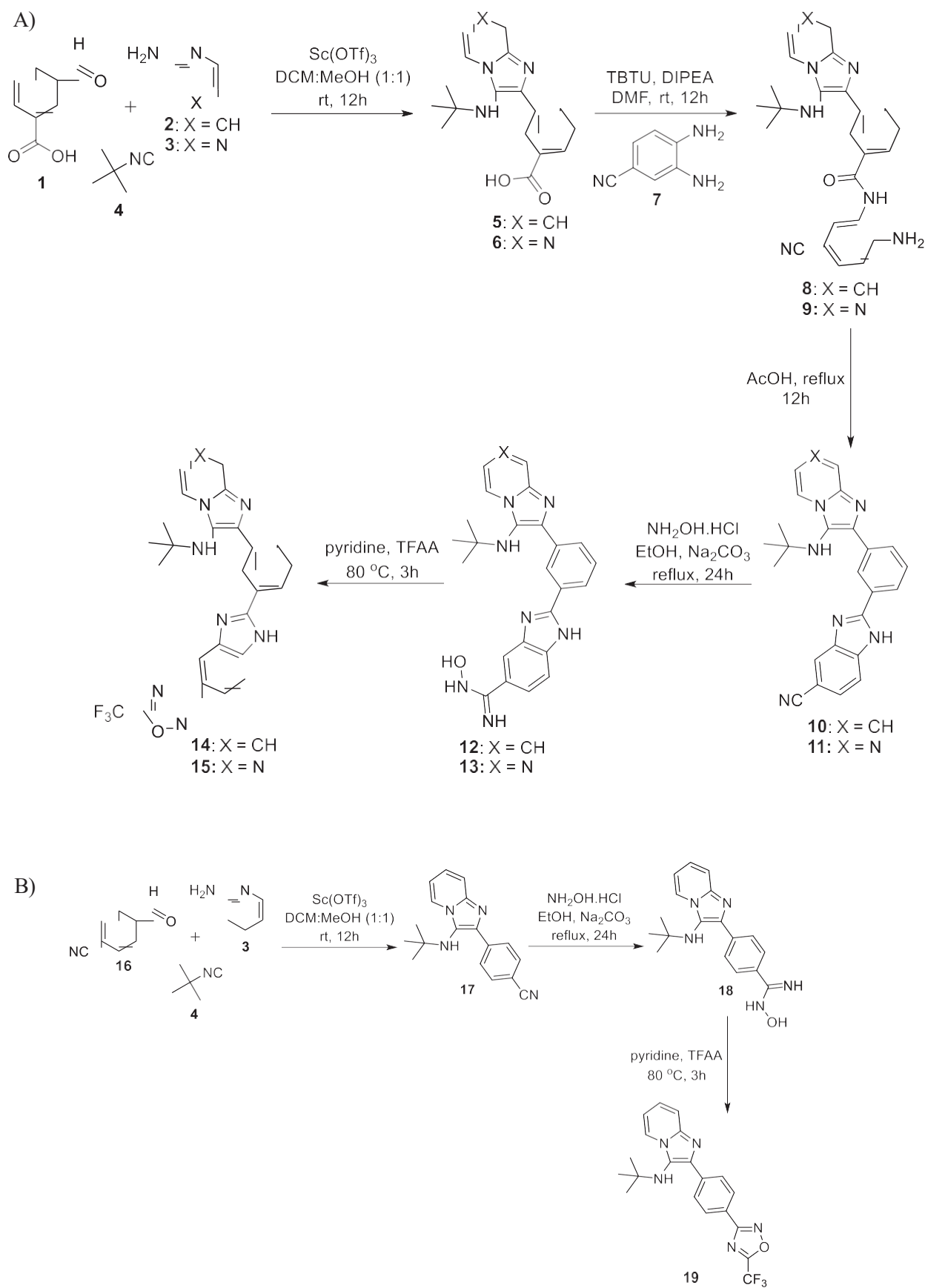
The maximum kinetic solubility of compound 28 in 2% DMSO/phosphate buffered saline was 36.1 mM. In the presence of NADPH, compound 28 demonstrated a half-life of 17.6 min in CD-1 mouse liver microsomes and a half-life of 7.1 min in pooled human liver microsomes at 37 °C. The compound was stable in microsomes from both species in the absence of NADPH under similar conditions. Compound 28

Table 1

In vitro ADME results for Compound 28.

Max. Aqueous Solubility* (μ M)	Stability, MLM** t _{1/2} (min)		Stability, HLM ^v t _{1/2} (min)		Human CYP450 Inhibition IC ₅₀ (nM)		
	+NADPH	–NADPH [‡]	+NADPH	–NADPH [‡]	3A4	2D6	2C9
36.1	17.6	94%	7.1	99%	233	>10,000	>10,000

*In 2% DMSO/phosphate buffered saline; **MLM = Mouse liver microsomes; ^vHLM = Human liver microsomes; [‡]Percent remaining after incubation for 60 min at 37 °C.



Scheme 1. Synthesis of (A) 14, 15 and (B) 19.

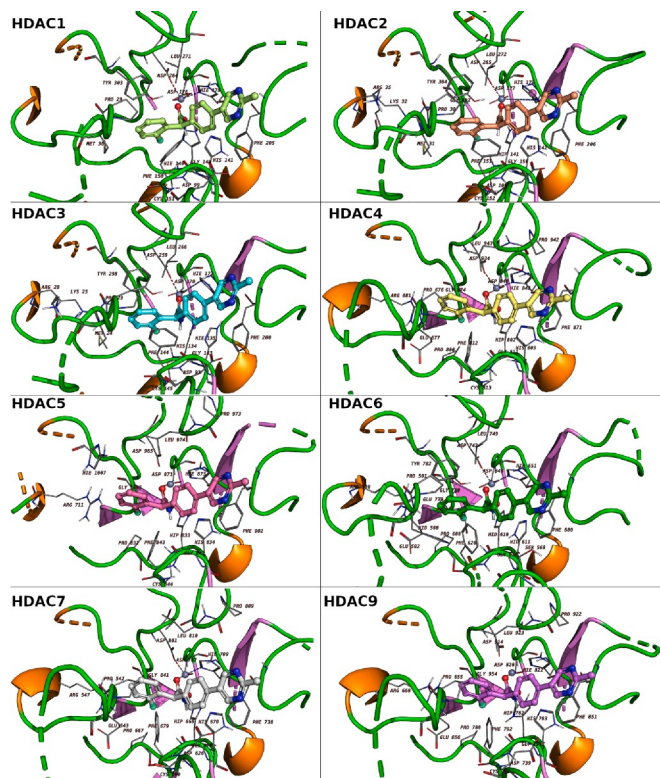
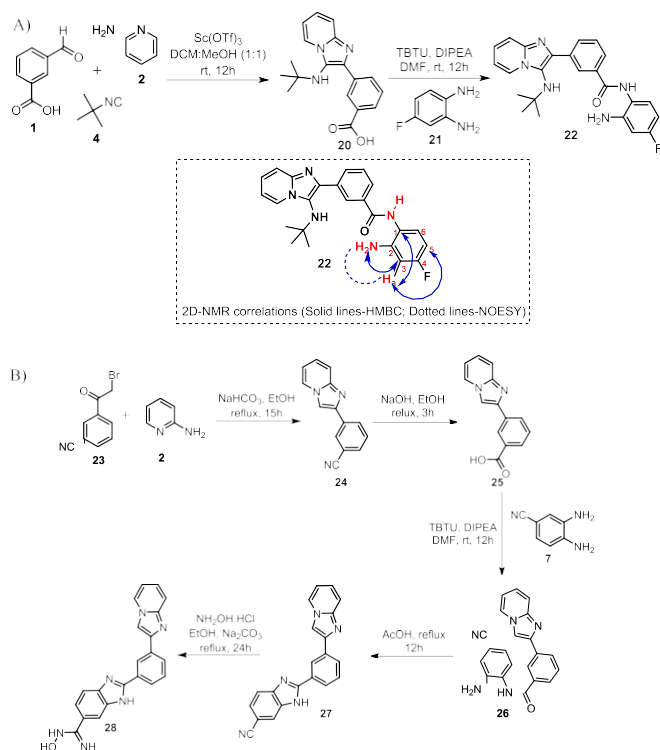


Fig. 2. Active site comparison of HDAC isoforms. HDAC 1 was used as the reference frame to align other structures. The RMSD values of HDAC2-7, and HDAC9 are 1.297 Å, 1.324 Å, 2.778 Å, 5.123 Å, 3.271 Å, 3.438 Å, and 4.858 Å, respectively.

displayed no inhibitory activity against human CYP450's 2D6 and 2C9 at concentrations up to 10 mM. The IC₅₀ value for human CYP450 3A4 was found to be 233 nM.

3.3. Biology

3.3.1. In-vitro biochemical HDAC inhibition assay

The potency and selectivity of the newly synthesized compounds against Class I (1, 2 & 3) and class IIa (4, 5, 7 & 9) HDACs were investigated using a cell-free HDAC inhibition assay. Vorinostat (SAHA) and MAD-1914 were examined as positive competitors. Results are presented in **Table 2**. Compound **28** was found to be an effective and selective inhibitor of HDAC 1 & HDAC2, with IC₅₀ values of 0.55 and 0.4 μM, respectively. Compound **22** demonstrated selectivity for HDAC3 and HDAC9, with IC₅₀ values of 2.12 and 1.30 μM, respectively. Compound **15** possessed a high degree of selectivity toward HDAC5 with an IC₅₀ of ca. 0.30 μM, whereas **14** selectively inhibited class II HDACs (HDAC4, HDAC5 and HDAC9), with the greatest selectivity seen for HDAC5 (IC₅₀ = 0.31 μM). Compound **19** also showed selectivity toward HDAC5, with an IC₅₀ value of 0.81 μM. It is noteworthy that the IC₅₀ of the positive control SAHA was higher than 10 μM for HDAC4,5,7 and 9, which is consistent with previously published results⁴⁷.

3.3.2. The effect of the new HDAC inhibitors on the expression and activity of various HDAC isozymes

To further validate the results of the HDAC enzymatic assay, the effects of compounds **14**, **15**, **19**, **21** and **28** on different HDACs were investigated in the MCF7 breast cancer cell line using gene expression and Western blot analysis (**Fig. 6**). As shown in **Fig. 5A**, **28** showed the most potent activity as an inhibitor of Class I HDACs (HDACs 1 and 2). Compound **28** inhibited gene expression by 2.2 fold for HDAC3 and 3.2 fold for HDAC1 compared to control cells. Its inhibition of class I HDACs gene expression was stronger than that seen for vorinostat. Compound **14** was also more effective than vorinostat at inhibiting Class I HDAC gene expression. Compounds **22** and **19** were found to be equally effective compared to vorinostat, while **15** actually increased the expression level of all class I HDACs as compared to control cells.

A similar pattern was observed for **28** when tested against the gene expression of Class IIa (HDAC 4, 5 and 7) (**Fig. 5B**), class IIb (HDAC 6 and 10) (**Fig. 5C**), class III (Sirtuin 1–7) (**Fig. 5D**) and class IV HDACs (HDAC 11) (**Fig. 5E**), indicating that **28** is the most potent inhibitor of the compounds tested, including vorinostat. Compounds **22**, **19** and **14** showed inhibition of these HDAC families as well, but with lower activity when compared to **28**. Compound **15** increased the expression of all HDAC families (**Figs. 5B–E**). All of our tested compounds demonstrated inhibitory activity on class III (Sirtuin 1–7) gene expression, with **28** being more active than **19**, **22**, or **14** (**Fig. 5D**). Interestingly, our compounds were effective at inhibiting gene expression for all seven sirtuins while vorinostat actually increased gene expression for SIRT2 and SIRT4. These data suggest that our compounds could be more effective than vorinostat at treating sirtuin-associated diseases, including cancer, HIV, metabolic disorders and pathologies associated with neurological diseases²¹.

3.3.3. Enhanced acetylation of histone proteins by the new HDAC inhibitors

Since HDACs de-acetylate histone proteins, HDACi's would be expected to increase levels of acetylated histones, we, therefore, examined the effects of our compounds on the acetylated forms of histones H2A, H3 and H4 in MCF7 cells by Western blot (**Fig. 6**). Compounds **15**, **19** and **28** significantly increased the degree of acetylation of all three histone proteins, whereas compounds **14** and **22** showed little effects on the acetylation of the three types of histones (**Fig. 6A and 6B**, **Fig. S16**).

Vorinostat also increased levels of acetylated histone proteins. The gene expression data revealed that **28** and **22** increased the degree of expression of histones H2A, H3 and H4 in a consistent manner. Interestingly, all compounds increased the level of H3 acetylation more than

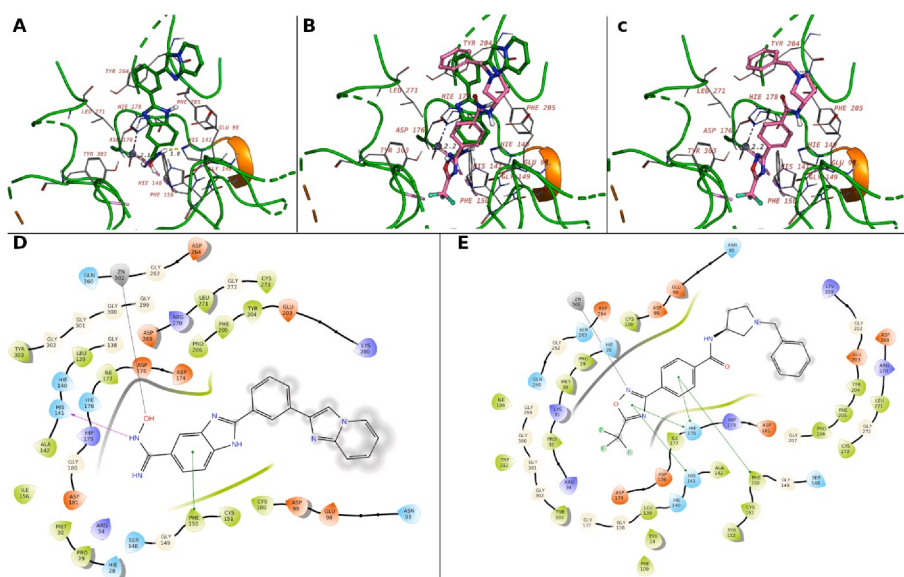


Fig. 3. Binding mode of **28** (A) and MAZ1914 (B) in HDAC1. A comparison of the binding modes of **28** and MAZ1914 in HDAC1 (C). The 2D interaction profile of **28** (D) and MAZ1914 (E) in HDAC1 showing different types of interactions with the surrounding amino acids. The protein is shown as cartoon, and ligands as sticks. The interacting amino acids are shown as lines.

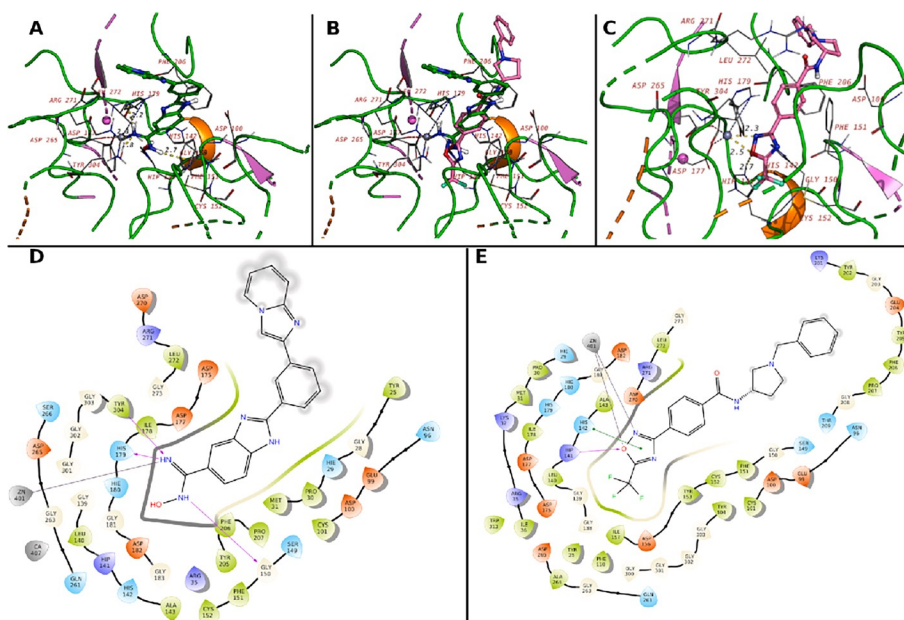


Fig. 4. Binding mode of **28** (A) and MAZ1914 (B) in HDAC2. A comparison of the binding modes of **28** and MAZ1914 in HDAC2 (C). The 2D interaction profile of **28** (D) and MAZ1914 (E) in HDAC2 showing different types of interactions with the surrounding amino acids. The protein is shown as cartoon, and ligands as sticks. The interacting amino acids are shown as lines.

vorinostat; however, the latter showed a greater effect on histone H2A compared to our compounds (Fig. 6C). This finding is consistent with previous reports, which showed that not all histones that are acetylated correlate with histone mRNA gene expression⁴⁸.

3.3.4. Anti-proliferative effects of the new HDAC inhibitors

HDAC inhibitors are known to prevent the proliferation of cancer cells. The effect of compounds **14**, **19**, **22** and **28** on the proliferation of breast cancer cell line MCF7 and lung cancer cell line A549, was studied using a sulforhodamine-B assay with doxorubicin and vorinostat (SAHA) as reference standards (Fig. 6D and E, Table 3). Compounds **14** and **19** showed a non-significant effect on cell survival in both cell lines. Compounds **22** and **28** were more effective than vorinostat in MCF7 cells and

compounds **28** was more effective than vorinostat in A549 cells. The IC₅₀ values of **28** were 2 and 0.2 μM for MCF7 and A549 cells respectively, while compound **22** demonstrated an IC₅₀ value of 0.7 μM in MCF7 cells. It is noteworthy that the IC₅₀ of vorinostat was >10 μM for both MCF7 and A549 cells, which is similar to earlier results^{49–50}. To better understand these findings, their effects of these compounds on the expression of several apoptotic markers in MCF7 cells were investigated. As shown in Fig. 7A and B, **15**, **28** and **22** reduced the expression level of the survival oncogenic protein C-MYC comparable to that of the positive control vorinostat.

These findings were in accordance with that seen from the gene expression data, which showed that **14**, **22** and **28** reduced the expression level of C-MYC more than vorinostat (SAHA) as shown in

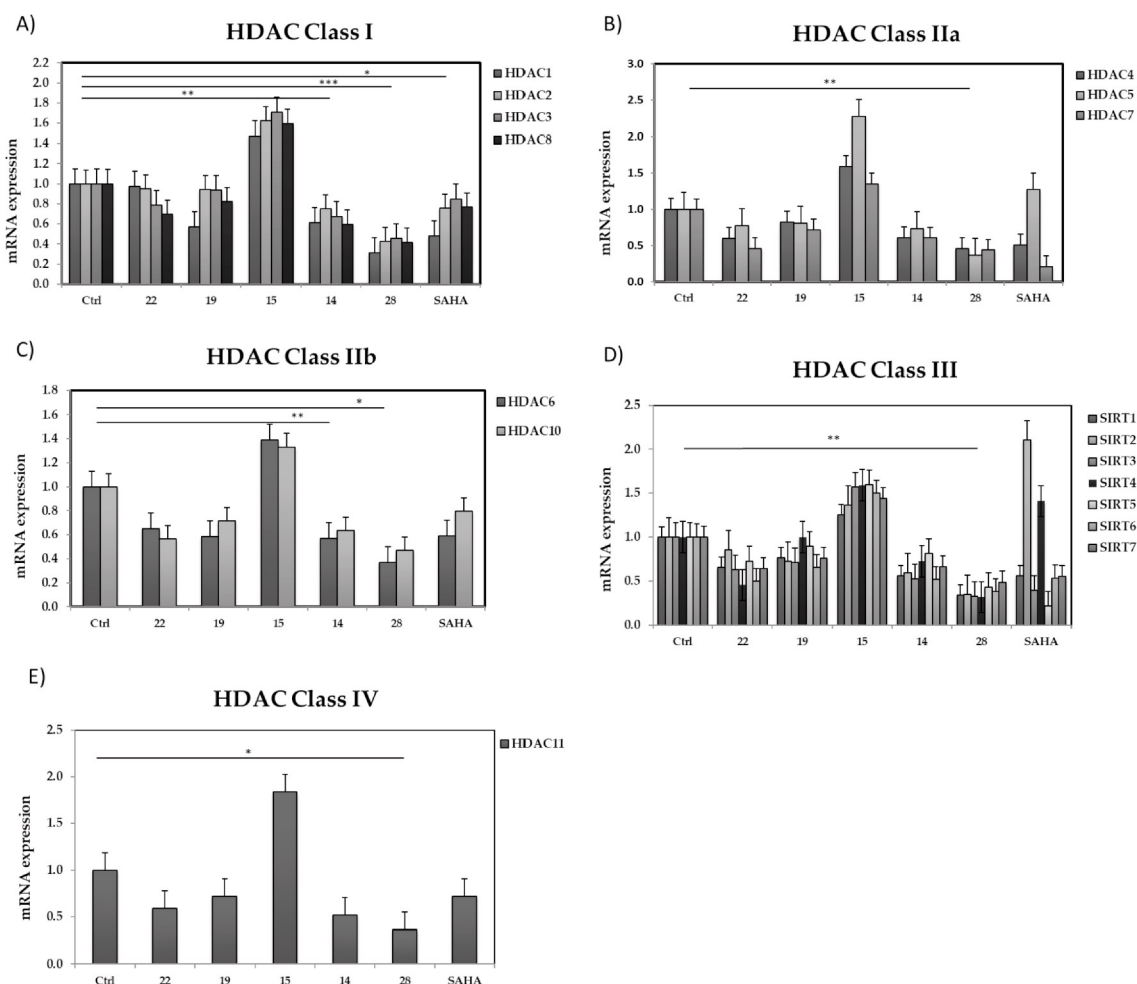


Fig. 5. Effect of the new compounds on gene expression of different HDAC families. MCF7 cells were treated with 3 μ M of each of the five compounds for 24 h and the effect of this treatment on the level of gene expression of different HDAC families was analyzed. Control cells treated with the vehicle (DMSO) were used as negative control, whereas cells treated with SAHA were used as positive control. (A) Class I HDACs, (B) Class IIa HDACs, (C) Class IIb HDACs, (D) Class III HDACs and (E) Class IV HDACs. * $p < 0.05$, ** $p < 0.01$ and *** $p < 0.001$.

Table 2

HDACs Inhibitors IC₅₀ compared to SAHA and MAZ1914 positive controls. IC₅₀ values are the average of three independent experiments each was carried out in triplicate.

Compound	IC ₅₀ (μ M)						
	HDAC1	HDAC2	HDAC3	HDAC4	HDAC5	HDAC7	HDAC9
14	>10	>10	>10	1.646	0.31	4.851	0.818
15	>10	>10	>10	8.00	0.3069	>10	>10
19	>10	>10	>10	3.584	0.8121	6.898	2.311
22	>10	>10	2.12	>10	12.4	6.1	1.3
28	0.55	0.40	>10	>10	>10	>10	>10
SAHA	0.010	0.013	0.019	>10	>10	>10	>10
MAZ1914	ND*	ND*	1.088	0.019	0.061	0.016	0.048

Shown are the means \pm SEM of at least three independent experiments each in triplicate. *ND = Not determined.

Fig. 7C. To further confirm the apoptotic effect of the new compounds, their effects on the expression of caspases 3/7 were studied. This study revealed that all compounds increased the expression of these caspases at levels that were either similar to (15, 19) or higher than vorinostat (14, 22, 28) (Fig. 7D). These findings were also observed in the gene expression studies. Furthermore, the results indicate that the new compounds led to a downregulation of the expression of the anti-apoptotic genes BCL3 and BCL2 compared to the control group. Compound 28 showed the greatest effect on downregulation of BCL2 and BCL3 expression, with 14, 19 and 22, downregulating BCL2 and BCL3

expression to a lesser extent, as shown in Fig. 7E. Its noteworthy to mention that vorinostat did not downregulate the expression of BCL3 (Fig. 7E).

To gain more insight into the anti-proliferative activity of the new compounds, their effect on the expression of NF- κ B was studied. NF- κ B is a transcription factor that regulates the expression of many genes involved in cell survival and the cellular response to stress. It is constitutively active in different types of tumors, activating anti-apoptotic genes and inhibiting caspase enzymes. Our compounds showed variable effects on the expression of NF- κ B genes. Compound 22 and

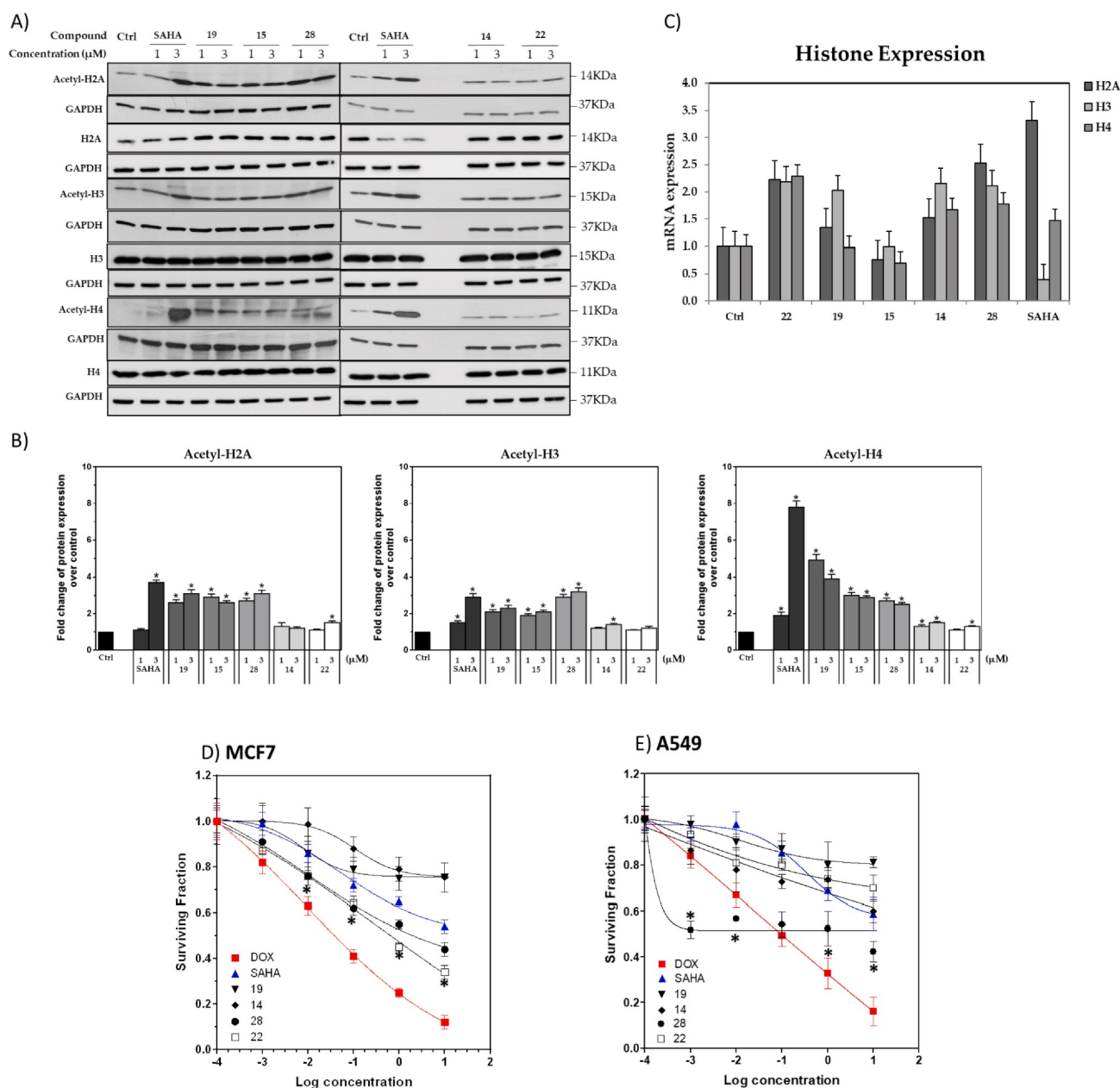


Fig. 6. Effect of compounds **14**, **15**, **19**, **22**, **28** and vorinostat (SAHA) on protein/mRNA expression of different acetylated histones. MCF7 cells were treated with 1 or 3 μ M of each of the five compounds and after 24 h the effect of this treatment on the level of protein expression of different acetylated histones was analyzed. Control cells treated with the vehicle (DMSO) were used as negative control, whereas cells treated with vorinostat were used as positive control. **(A)** Immunoblotting of acetylated histones H2A, H3 and H4, **(B)** Quantification of band intensities of the indicated proteins. Each protein visualized on a blot was normalized to the corresponding GAPDH as a loading control. Full-length blots are presented in Supplementary Fig. S20. **(C)** mRNA level of H2A, H3 and H4 was analyzed in MCF7 cells treated with 3 μ M of each of the six compounds. **(D&E)** Anti-proliferative effects of compounds **14**, **15**, **19**, **22**, **28**, vorinostat (SAHA) and doxorubicin (DOX) on breast cancer (MCF7) and lung (A549) cancer cell lines. Cells were treated with different concentrations of each of the five compounds (0.001–10 μ M) for 48 h. The fraction of cells remaining viable at the end of the treatment period was analyzed by sulf-rhodamine-B assay. Control cells were treated with DMSO as a negative control. Vorinostat (SAHA) and doxorubicin were used as positive controls. * $p < 0.05$ versus DMSO treated cells.

vorinostat downregulated the expression of NF- κ B1, RELA (P65) and RELB while upregulating the expression NF- κ B2 (p52). However, **19** showed a slight reduction in NF- κ B gene expression. The highest reduction in NF- κ B gene expression was observed with **14** and **28**, including effects on NF- κ B2, which was also upregulated by vorinostat. On the other hand, **15** enhanced the expression of all measured NF- κ B genes (Fig. 7F). Taken together, these data indicate that the five new compounds, in particular **22** and **28**, showed promising anti-proliferative effects on MCF7 cells compared to vorinostat through modulating the expression of cell survival and apoptotic genes.

3.3.5. The effect of the new compounds on cell cycle regulation

HDAC inhibitors like vorinostat possess many cellular effects either through enhanced acetylation of histone proteins and subsequent changes in gene expression or elevated acetylation of non-histone targets. Therefore, to further validate the anticancer activities of our compounds, we investigated whether they regulate cell cycle in MCF7 breast cancer cells. The results are summarized in Fig. 8. After treatment for 4 h, vorinostat (SAHA), **14** and **15** induced a significant arrest of cells at G1/S phase, whereas **19** and **22** induced G2/M arrest. After 24 h of treatment, **15**, **19**, **22** and vorinostat (SAHA) induced arrest in G2/M

Table 3

Antiproliferative IC₅₀ values of compounds **14**, **19**, **22**, **28**, vorinostat and doxorubicin in MCF7 and A549 cells.

Compound	IC ₅₀ (μM)	
	MCF7	A549
14	>10	>10
19	>10	>10
22	0.7 ± 0.03	>10
28	2 ± 0.09	0.2 ± 0.001
Vorinostat (SAHA)	>10	>10
Doxorubicin	0.038 ± 0.005	0.09 ± 0.008

Shown are the means ± SEM of at least three independent experiments each in triplicate.

phases (Fig. 8A and 8B). At different time points (24 h, 48 h and 72 h), variable percentages of subG1 cells (indicative of apoptosis), were detected for all compounds except for **14**. At the 24 h time point, the induced fraction of subG1 by **19** was higher than that seen with vorinostat (SAHA), whereas at the 48 h and 72 h time points, vorinostat was more effective than the new compounds in the induction of subG1 cells (Fig. 8C). These findings agree with the gene expression results which indicated that our compounds affected the expression of many genes involved in cell cycle progression at different levels. Compound **28** was the most effective inhibitor of cell cycle progression genes, followed by **14** and **19** (Fig. 8D).

Our compounds also decreased the expression of the cyclin-dependent kinases CDK2, CDK4 and CDK6, which are involved in the progression of cells from G1 to S phase. Additionally, the compounds also reduced the expression of CDK1, which regulates the progression of cells from G2 to M phase. Moreover, our compounds downregulate the expression of both E2F1 and RB1 genes, which are known to be cell cycle regulators. Interestingly, vorinostat showed the most effective inhibition of E2F1. However, of the compounds under investigation, **28** showed the most consistent downregulation of all cell cycle progression genes studied. Collectively, these results suggest that the new compounds induce cell cycle arrest through downregulation of cell cycle genes.

4. Discussion

There are 18 known histone deacetylase isozymes, which are clustered into four families based on their homology (Classes I, IIa/IIb, III and IV). They differ in their cellular localization, associated cofactors and their physiological functions. The FDA has approved two HDACi (vorinostat and romidespin) for the treatment of cutaneous T-cell lymphoma (CTCL) either as a single therapy or in combination with other anti-cancer drugs. Both of these drugs are pan-inhibitors of all HDACs. More recently, a number of more potent and selective HDACi's have been introduced in clinical trials as potential anti-cancer agents^{51–52}. The clinically available HDACi's are used for hematologic malignancies; however, the use of HDACi's for the treatment of solid malignancies such

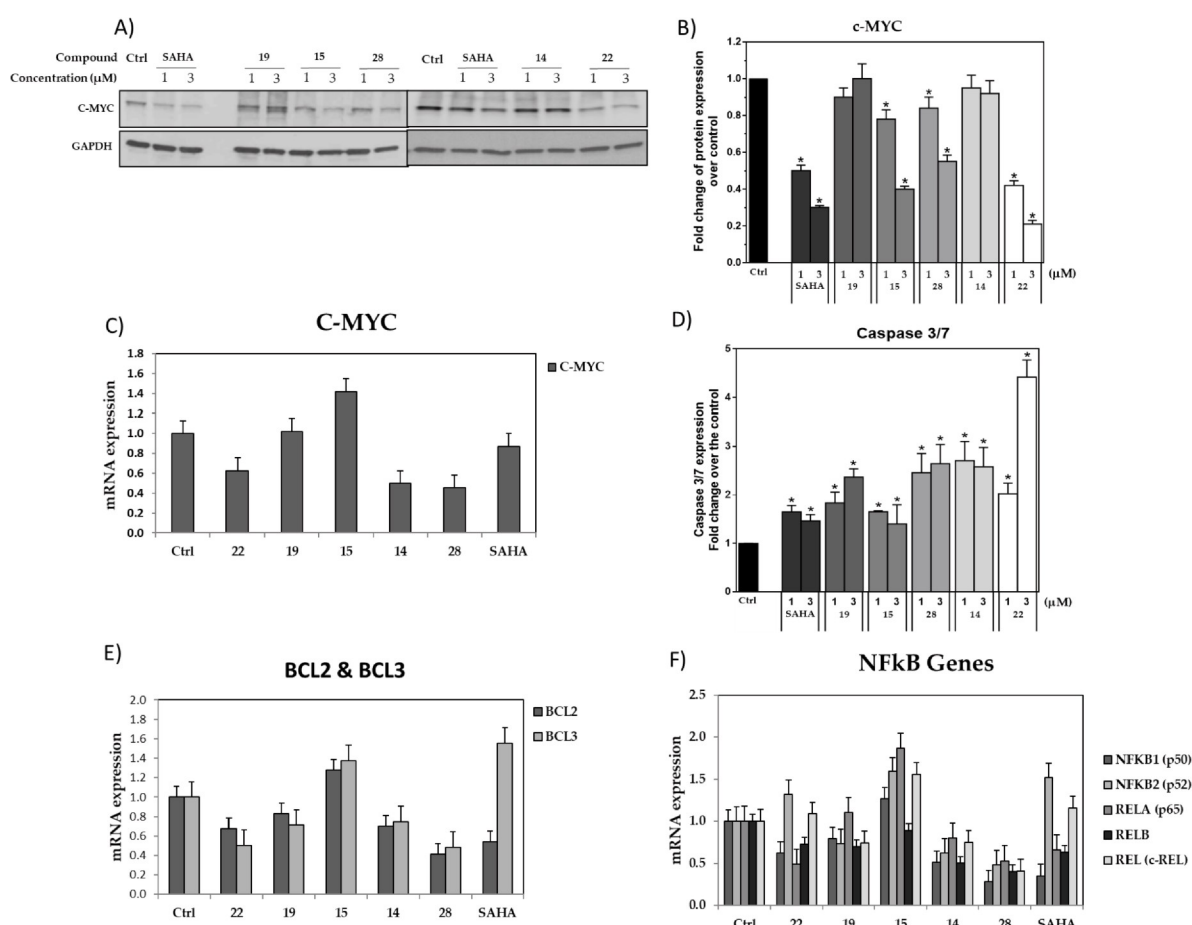


Fig. 7. Effect of compounds **14**, **15**, **19**, **22**, **28** and vorinostat (SAHA) on protein/gene expression of different apoptotic markers. (A) Western blot analysis of C-MYC protein expression after treatment of MCF7 cells with 1 or 3 μM of each of the 5 compounds and SAHA as positive control. (B) Quantification of C-MYC protein expression normalized to GAPDH. (C) Analysis of C-MYC gene expression in MCF7 cells treated with 1 μM of each of the 5 compounds and SAHA as positive control. (D) Caspase 3/7 activity in MCF7 cells treated with 1 or 3 μM of each of the 5 compounds and SAHA as positive control. (E) Analysis of BCL2 and BCL3 gene expression after treatment of MCF7 with 3 μM of each of the 5 compounds and SAHA as positive control. (F) Analysis of NFκB genes expression after treatment of MCF7 with 3 μM of each of the 5 compounds and SAHA as positive control. Control cells were treated with DMSO only. * p < 0.05 versus DMSO treated cells.

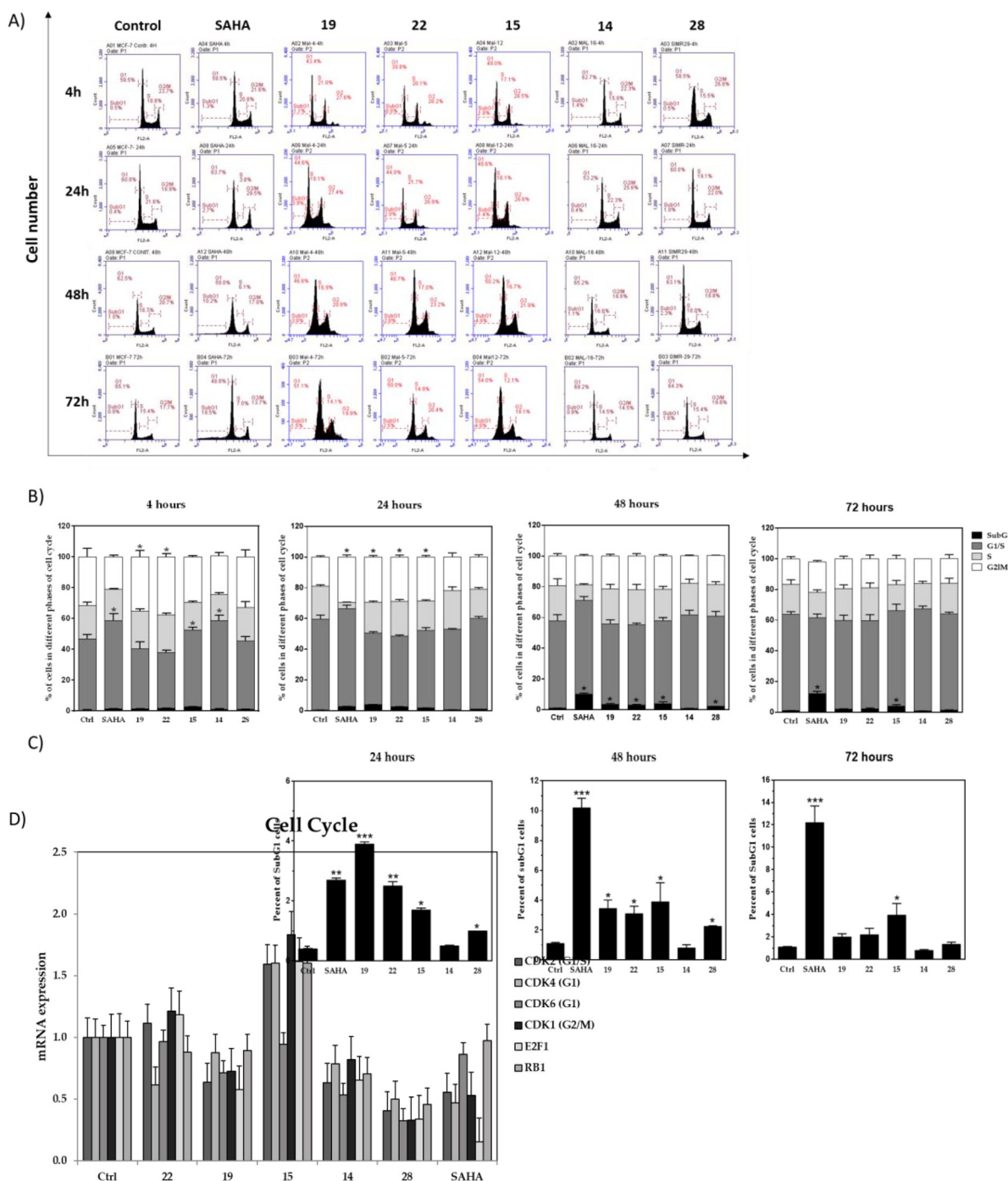


Fig. 8. Effect of the new compounds on cell cycle distribution in MCF7 cells. (A) Flow cytometry chart of cell cycle distribution of MCF7 cells treated for different time intervals (4–72 h) with 1 μ M of each of the 5 compounds and SAHA as positive control. (B) Quantification of cell cycle distribution at different time intervals. (C) Quantification of subG1 cells at 24, 48 and 72 h time points. (D) Gene expression analysis of cell cycle markers (CDK 1, 2, 4, 6, E2F1 and RB1) after treatment of MCF7 with 3 μ M of each of the 5 compounds and SAHA as positive control. Control cells were treated with DMSO only. * $p < 0.05$ versus DMSO treated cells.

as breast cancer has not been pursued as aggressively despite a correlation between elevated levels of HDACs and tumor aggressiveness, expression of hormone receptors (ER, PR and HER2) and the response of breast cancer cells to hormonal therapy was previously extensively studied^{33–36}.

In the present study, we identified a new class of selective HDAC inhibitors as potential anticancer lead drug candidates. These compounds were discovered while screening an in-house compound collections containing various core scaffolds and substitution patterns against representatives of zinc-dependent HDAC classes (Class I: HDACs

1, 2, and 3; Class IIa: HDACs 4, 5, 7 and 9). Based on the results obtained with compound **28**, the chemical scaffold possesses moderate kinetic aqueous solubility (maximum kinetic solubility of **28** in 2% DMSO/PBS = 36.1 μ M) that was adequate for the concentration range tested in the biological assays (0.001–10 μ M). Compound **28** demonstrated moderate stability in mouse liver microsomes ($t_{1/2}$ = 17.6 min) and lower stability in human liver microsomes ($t_{1/2}$ = 7.1 min). The compound was stable when incubated with mouse and human liver microsomes in the absence of NADPH, suggesting that P450-mediated oxidative metabolism is the primary metabolic event in the liver microsomal fraction. Compound **28**

showed no inhibition of the human metabolizing enzymes CYP2D6 and CYP2C9 at concentrations up to 10 μ M. The compound did demonstrate some inhibition of CYP3A4 (IC_{50} = 233 nM). This result is in contrast to vorinostat, which was reported to show no inhibitory activity against multiple human CYP450 enzymes at concentrations up to 75 μ M, and suggests the possibility of drug-drug interactions between **28** and other compounds that either inhibit or are metabolized by CYP3A4.

The biological effects of hits on MCF7 cells (derived from solid tumors) was then investigated. Our evaluation included enzymatic inhibition, effects on gene expression and whole cell anti-proliferative assays. The results of these assays are summarized in Tables 2–3 and Figs. 5–8. The HDAC inhibitory assay provided valuable information on the structure–activity relationship. Strikingly, two of the compounds were found to be potent HDAC5 inhibitors (**14** and **15**) with IC_{50} values ca. 300 nM (Table 2). Compound **15** was found to be 33-fold more selective toward HDAC5 compared to other HDACs studied. The most potent HDAC1 and HDAC2 inhibitor was compound **28**, with an IC_{50} value of 550 and 400 nM, respectively. Compound **28** was found to be 44-fold more selective toward HDACs1 and 2 compared to other HDACs studied. At this stage, some structure–activity conclusions can be made. Compounds with a trifluoromethyloxadiazole (TFMO)-benzimidazole cap group anchored on imidazo-azine isophthalic acid derivative (**14** and **15**) displayed strong potency and appreciable selectivity in the enzymatic HDAC assay toward HDAC5, and showed better potency (>33-fold) compared to the FDA-approved drug vorinostat. Interestingly, replacing the *tert*-butyl group of **14** and **15** with a hydrogen and substituting the trifluoromethyloxadiazole ring with *N*-hydroxyl amidine (as in **28**) diminished the activity toward HDAC5. The latter change however, enhanced the selectivity and potency of **28** toward HDAC1 and 2 by >44-fold. Furthermore, the fluoro-phenylene diamine group present in compound **22**, was found to enhance the potency toward HDAC3 and HDAC9 compared to other HDACs studied. These results could be rationalized based on the biased functional groups present in these motifs. For example, the TFMO group has been reported to possess selectivity towards Class IIa HDACs, whereas the amino/hydroxy amidine moieties enhances the selectivity towards class I HDACs⁵⁷. Most of the known HDAC inhibitors possess a common pharmacophore which comprises a zinc-chelating group in the active site, a linker that accesses the hollow of the active site and a group that networks with the external surface⁵⁷. With this in mind, the observed selectivity of our compounds against the different HDACs isoforms, might be due to the novel system comprising a trifluoromethyloxadiazole (TFMO) group appended to an imidazopyridine-isophthalic acid chromophore structure.

To further validate the HDACi inhibitory activity of our compounds, their cytotoxic effects was studied. Notably, compounds **22** and **28** exhibited appreciable anti-proliferative activity and displayed higher cytotoxicity when compared to the reference compound vorinostat, with IC_{50} values in MCF7 cells of 0.7 and 2.0 μ M, respectively. Gene expression analysis confirmed the inhibitory effects of the five new compounds on various HDAC isozymes. However, some variations in the selectivity of the new compounds towards different HDACs were observed when comparing the enzymatic assay results with gene expression results. For example, **28** showed a significant decrease in the gene expression mediated by all HDACs, while in the enzymatic assay significant selectivity was only observed toward HDAC1 and HDAC2. Similar differences between mRNA level and protein levels/activity for HDACs have been observed within different pathways, including sensory and neural pathways^{58–59}. In addition, studies have shown that certain histones such as H3 display a negative correlation between mRNA and protein expression⁶⁰. This might be due to the fact that the acetylation of H3 can also lead to other post-translation modifications such as methylation. For example, a 2015 study reported that trimethylation of lysine36 on H3 restricted gene expression, resulting in a discrepancy between H3 mRNA and protein expression⁶⁰.

It is noteworthy to mention that, four of the compounds (**14**, **19**, **22**, and **28**) induced down-regulation of the gene expression of the 7 SIRT

enzymes (Class III HDACs) with compound **28** being the most potent. This may suggest that the observed anti-proliferation effects of the tested compounds might be due to SIRT inhibition. Class III HDACs have already been shown to be overexpressed in some types of cancers and are considered as an attractive target for cancer therapy⁶¹. To this end, compound **28** also inhibited the gene expression of other HDAC classes (Classes I, IIa, IIb and IV). This is not in line with the biochemical data in which compound **28** showed a potent inhibition of class I HDACs only. This is mainly because the two assays (the biochemical and the gene expression assays) are measuring two different endpoints: the biochemical assay measures the effects on the enzymes activity whereas the gene expression measures the mRNA level of the genes. The anti-proliferative activity of compound **28** against the two tested cell lines may support this hypothesis that compound **28** inhibited the gene expression of HDACs rather than their activities.

HDAC inhibition alters the balance between histone acetyl transferase activity and HDAC activity, resulting in elevated acetylation of histone proteins. Acetylation of histone lysine residues is associated with an open chromatin structure and transcriptional activation of many genes involved in signal transduction, DNA repair, cell cycle regulation and cell death pathways such as apoptosis, autophagy and cell senescence⁵⁰. As expected, three of our compounds (**15**, **19** and **28**), showed a significant increase in the levels of acetylation of various histones, which confirms their HDACs inhibitory effects. These findings are in line with a previous report from Bali et al⁶² that indicated the enhancement of acetylation of H3 and H4 after treatment of breast cancer cells with the HDAC inhibitor vorinostat. Interestingly, compounds **15**, **19** and **28** induced a lower acetylation of histone H4 compared to vorinostat. This result might be due to the potent HDAC inhibitory activity of vorinostat toward HDACs 1, 2 and 3 compared to the three compounds (Table 2)⁶³.

Numerous reports indicate that HDACi's possess the ability to halt the proliferation of cancer cells when used alone or in combination with other anti-cancer drugs^{64–65}. Most of these reports discuss the anti-cancer activities of HDACi on liquid malignancies. There are relatively few reports of studies examining the anti-cancer activity of HDACi's on solid malignancies. To this point, treatment with two of our compounds, **22** and **28**, resulted in a large reduction in the survival of MCF7 breast cancer cells and the non-small cell lung cancer cells A549 (only compound **28**) compared to treatment with vorinostat and doxorubicin. This enhanced anti-cancer activity can only partially be attributed to the compounds' HDAC inhibitory effects since **14** and **15** did not exert significant anti-proliferative effects. The reasons for these results are not clear at present but may be the result of the effects of **22** and **28** on other proteins in addition to HDACs.

To further validate the anti-cancer activity of our compounds, we examined their effects on the expression of apoptosis and cell cycle progression markers. The balance between survival proteins such as C-MYC, BCL2, BCL3 and NFkB and death proteins such as caspases3 and 7 determines the fate of cancer cells treated with anticancer therapeutics. NF-kB is a transcription factor that regulates the expression of many genes involved in cell survival and cellular response to stress. It is constitutively active in different types of tumors, activating anti-apoptotic genes and inhibiting caspase enzymes. BCL3 is a key member of the NF-kB signaling cascade and is known to be involved in regulating many cellular functions, including survival, proliferation, inflammation and immune response. Increased cellular proliferation or survival is associated with BCL3 expression and activation⁶⁶. Furthermore, BCL3 transcriptional repressor function has been shown to play a role in regulating immune responses and in the development and activation of immune cells⁶⁷. The fact that the expression of BCL3 is downregulated in cancer cells indicates a modification in the immune response as well as survival and proliferation outcomes of cell signaling. In our studies the anti-apoptotic gene BCL2 was overexpressed in control cells but was downregulated in cells treated with our compounds (Fig. 7E). BCL2 expression is known to be upregulated in many primary tumors. Downregulation of BCL2 results in reduced proliferation and

pro-apoptotic effects in these tumors. C-MYC is another survival protein that is overexpressed in different types of liquid and solid malignancies and has been reported as a known target of HDACi⁶⁸. The upregulation of caspase7 and downregulation of C-MYC, BCL2, BCL3 and NFkB by our compounds support their role in enhancing cells apoptotic machinery, which further explains the anticancer effect of our new HDACi's against solid malignancies such as, MCF7 breast cancer cells. These results are consistent with previous findings^{65,69-71}.

Cell cycle arrest is another effect of HDAC inhibition⁶⁴. TA significant increase in the fraction of MCF7 cells in G1/S and G2/M phases was detected after treatment with our compounds. This effect was accompanied by a downregulation in the expression of proteins involved in cell cycle progression such as E2F1, RB1 and cyclin-dependent kinases (CDKs 1, 2, 4 and 6). These results are also in agreement with previous findings which indicated a reduction in the levels of cyclins and CDKs after treatment of cancer cells with HDACi's^{65,72}.

Inhibition of HDACs (resulting in increased acetylation of histone lysine residues) can explain the biological effects of our new compounds (anti-proliferation, apoptosis and cell cycle effects), but does not fully explain the enhanced activity seen with **22** and **28** compared to that observed for **14**, **15** and **19**. It is possible that selective effects on other proteins and/or signaling pathways may be occurring. This hypothesis will be tested using genetic knockout/knockdown and overexpression of individual HDACs and will be the subject of future reports.

In summary, we have discovered a novel series of selective imidazopyridine-based HDAC inhibitors. The data presented in this article demonstrated that the peptidomimetic-based core structure represents a new class of selective HDAC inhibitors with good activity against MCF7 solid tumor cells. Additionally, we have reported a unique class of chemical probes that inhibits class IIa HDAC containing a trifluoromethoxydiazolyl (TFMO) moiety as a nonchelating metal-binding group. These novel chemical probes forms the foundation for the discovery of selective inhibitors of these isozymes.

Furthermore, our new compounds upregulated the expression of caspase7 whereas they downregulated the expression of C-MYC, BCL2, BCL3 and NFkB. Moreover, the new compounds downregulated the expression of cell cycle progression proteins E2F1, RB1 and cyclin-dependent kinases (CDKs 1, 2, 4 and 6). These findings suggest that our compounds should be effective in treating solid malignancies.

Taken together, the biochemical, Western-blotting, whole cell assays and transcriptomic studies indicated that this novel series holds promise for further development as potential lead drug candidates for the treatment of cancerous disease states, including solid tumors.

CRedit authorship contribution statement

Raafat El-Awady: Conceptualization, Data curation, Supervision. **Ekrum Saleh:** Methodology, Writing - review & editing. **Rifat Hamoudi:** Methodology, Formal analysis, Writing - review & editing. **Wafaa S. Ramadan:** Methodology, Data curation. **Ralph Mazitschek:** Methodology. **Manal A. Nael:** Molecular modeling, Writing - original draft, Writing - review & editing. **Khaled M. Elokely:** Molecular modeling, Writing - original draft. **Magid Abou-Gharbia:** Writing - original draft. **Wayne E. Childers:** Writing - review & editing. **Vunnam Srinivasulu:** Methodology. **Lujain Aloum:** Methodology, Data curation. **Varsha Menon:** Methodology, Data curation. **Taleb H. Al-Tel:** Conceptualization, Writing - review & editing, Supervision, Project administration, Funding acquisition.

Declaration of Competing Interest

The authors declare that they have no known competing financial interests or personal relationships that could have appeared to influence the work reported in this paper.

Acknowledgments

This work was supported by generous grants from the TerryFox Foundation (grant number 120403) and the Research Funding Department at the University of Sharjah (grant number 1801110125-P).

Appendix A. Supplementary material

Supplementary data to this article can be found online at <https://doi.org/10.1016/j.bmc.2021.116251>.

References

- Baxter E, Windloch K, Gannon F, Lee JS. Epigenetic regulation in cancer progression. *Cell Biosci.* 2014;4:45–45. doi: [10.1186/2045-3701-4-45](https://doi.org/10.1186/2045-3701-4-45).
- Sharma S, Kelly TK, Jones PA. Epigenetics in cancer. *Carcinogenesis.* 2010;31(1):27–36. <https://doi.org/10.1093/carcin/bgp220>.
- Grunstein M. Histone acetylation in chromatin structure and transcription. *Nature.* 1997/09/01 1997;389(6649):349–352. <https://doi.org/10.1038/38664>.
- Marks PA, Rifkin RA, Richon VM, Breslow R, Miller T, Kelly WK. Histone deacetylases and cancer: causes and therapies. *Nat Rev Cancer.* 2001/12/01 2001;1(3):194–202. <https://doi.org/10.1038/35106079>.
- Ropero S, Esteller M. The role of histone deacetylases (HDACs) in human cancer. *Mol Oncol.* 2007;1(1):19–25. <https://doi.org/10.1016/j.molonc.2007.01.001>.
- Seto E, Yoshida M. Erasers of histone acetylation: the histone deacetylase enzymes. *CSH Perspect Biol.* 2014;6(4), a018713. <https://doi.org/10.1101/cshperspect.a018713>.
- Sathishkumar C, Prabu P, Balakumar M, et al. Augmentation of histone deacetylase 3 (HDAC3) epigenetic signature at the interface of proinflammation and insulin resistance in patients with type 2 diabetes. *Clin Epigenetics* 2016;8:125–125. doi: [10.1186/s13148-016-0293-3](https://doi.org/10.1186/s13148-016-0293-3).
- Bradner JE, Mak R, Tanguturi SK, et al. Chemical genetic strategy identifies histone deacetylase 1 (HDAC1) and HDAC2 as therapeutic targets in sickle cell disease. *Proc Natl Acad Sci U S A.* 2010;107(28):12617–12622. <https://doi.org/10.1073/pnas.1006774107>.
- Suraweera A, O'Byrne KJ, Richard DJ. Combination Therapy With Histone Deacetylase Inhibitors (HDACi) for the Treatment of Cancer: Achieving the Full Therapeutic Potential of HDACi. *Front Oncol.* 2018;8:92. <https://doi.org/10.3389/fonc.2018.00092>.
- Diyabalanage HVK, Grand ML, Hooker JM. Combination therapy: histone deacetylase inhibitors and platinum-based chemotherapeutics for cancer. *Cancer Lett.* 2013;329(1):1–8. <https://doi.org/10.1016/j.canlet.2012.09.018>.
- Mann BS, Johnson JR, Cohen MH, Justice R, Pazdur R. FDA approval summary: vorinostat for treatment of advanced primary cutaneous T-cell lymphoma. *Oncologist.* 2007;12(10):1247–1252. <https://doi.org/10.1634/theoncologist.12-10-1247>.
- Frye R, Myers M, Axelrod KC, et al. Romidepsin: a new drug for the treatment of cutaneous T-cell lymphoma. *Clin J Oncol Nurs.* 2012;16(2):195–204. <https://doi.org/10.1188/12.cjon.195-204>.
- Al-Tel TH, Al-Qawasmeh RA. Post Groebke-Blackburn multicomponent protocol: synthesis of new polyfunctional imidazo[1,2-a]pyridine and imidazo[1,2-a]pyrimidine derivatives as potential antimicrobial agents. *Eur J Med Chem.* 2010/12// 2010;45(12):5848–5855. <https://doi.org/10.1016/j.ejmech.2010.09.049>.
- Liu J, Zhou J, He F, et al. Design, synthesis and biological evaluation of novel indazole-based derivatives as potent HDAC inhibitors via fragment-based virtual screening. *Eur J Med Chem* 2020/04/15/ 2020;192:112189. doi: <https://doi.org/10.1016/j.ejmech.2020.112189>.
- Futatsugi K, Kung DW, Orr STM, et al. Discovery and Optimization of Imidazopyridine-Based Inhibitors of Diacylglycerol Acyltransferase 2 (DGAT2). *J Med Chem.* 2015/09/24 2015;58(18):7173–7185. <https://doi.org/10.1021/acs.jmedchem.5b01006>.
- Song Q, Li M, Fan C, et al. A novel benzamine lead compound of histone deacetylase inhibitor ZINC24469384 can suppresses HepG2 cells proliferation by upregulating NR1H4. *Sci Rep* 2019/02/20 2019;9(1):2350. doi: [10.1038/s41598-019-39487-6](https://doi.org/10.1038/s41598-019-39487-6).
- Bradner JE, West N, Grachan ML, et al. Chemical phylogenetics of histone deacetylases. *Nat Chem Biol.* 2010;6(3):238–243. <https://doi.org/10.1038/nchembio.313>.
- Saleh EM, El-awady RA, Eissa NA, Abdel-Rahman WM. Antagonism between curcumin and the topoisomerase II inhibitor etoposide: a study of DNA damage, cell cycle regulation and death pathways. *Cancer Biol Ther.* 2012;13(11):1058–1071. <https://doi.org/10.4161/cbt.21078>.
- El-Awady RA, Saleh EM, Dahm-Daphi J. Targeting DNA double-strand break repair: is it the right way for sensitizing cells to 5-fluorouracil? *Anticancer Drugs.* 2010;21(3):277–287. <https://doi.org/10.1097/CAD.0b013e328334b0ae>.
- El-Awady RA, Saleh EM, Ezz M, Elsayed AM. Interaction of celecoxib with different anti-cancer drugs is antagonistic in breast but not in other cancer cells. *Toxicol Appl Pharmacol.* 2011/09/15/ 2011;255(3):271–286. <https://doi.org/10.1016/j.taap.2011.06.019>.
- Muhammad JS, Jayakumar MN, Elemam NM, et al. Gasdermin D Hypermethylation Inhibits Pyroptosis And LPS-Induced IL-1 β Release From NK92 Cells. *Immunotargets Ther.* 2019;8:29–41. <https://doi.org/10.2147/ITT.S219867>.

- 22 Turnbull RE, Fairall L, Saleh A, et al. The MiDAC histone deacetylase complex is essential for embryonic development and has a unique multivalent structure. *Nat Commun* 2020;06/26 2020;11(1):3252. doi: [10.1038/s41467-020-17078-8](https://doi.org/10.1038/s41467-020-17078-8).
- 23 Yu W, Liu J, Yu Y, et al. Discovery of ethyl ketone-based HDACs 1, 2, and 3 selective inhibitors for HIV latency reactivation. *Biorganic Med Chem Lett*. 2020;30(13), 127197. <https://doi.org/10.1016/j.bmcl.2020.127197>.
- 24 Watson PJ, Fairall L, Santos GM, Schwabe JWR. Structure of HDAC3 bound to co-repressor and inositol tetraphosphate. *Nature*. 2012/01/01 2012;;481(7381): 335–340. <https://doi.org/10.1038/nature10728>.
- 25 Luckhurst CA, Aziz O, Beaumont V, et al. Development and characterization of a CNS-penetrant benzhydryl hydroxamic acid class IIa histone deacetylase inhibitor. *Biorganic Med Chem Lett*. 2019;29(1):83–88. <https://doi.org/10.1016/j.bmcl.2018.11.009>.
- 26 Hai Y, Christianson DW. Histone deacetylase 6 structure and molecular basis of catalysis and inhibition. *Nat Chem Biol*. 2016;12(9):741–747. <https://doi.org/10.1038/nchembio.2134>.
- 27 Schuetz A, Min J, Allali-Hassani A, et al. Human HDAC7 harbors a class IIa histone deacetylase-specific zinc binding motif and cryptic deacetylase activity. *J Biol Chem*. 2008;283(17):11355–11363. <https://doi.org/10.1074/jbc.M707362200>.
- 28 Jones DT, Swindells MB. Getting the most from PSI-BLAST. *Trends Biochem Sci*. 2002; 27(3):161–164. [https://doi.org/10.1016/s0968-0004\(01\)02039-4](https://doi.org/10.1016/s0968-0004(01)02039-4).
- 29 Bottomley MJ, Lo Surdo P, Di Giovine P, et al. Structural and functional analysis of the human HDAC4 catalytic domain reveals a regulatory structural zinc-binding domain. *J Biol Chem*. 2008;283(39):26694–26704. <https://doi.org/10.1074/jbc.M803514200>.
- 30 Jacobson MP, Pincus DL, Rapp CS, et al. A hierarchical approach to all-atom protein loop prediction. *Proteins*. 2004;55(2):351–367. <https://doi.org/10.1002/prot.10613>.
- 31 Jacobson MP, Friesner RA, Xiang Z, Honig B. On the role of the crystal environment in determining protein side-chain conformations. *J Mol Biol*. 2002;320(3):597–608. [https://doi.org/10.1016/s0022-2836\(02\)00470-9](https://doi.org/10.1016/s0022-2836(02)00470-9).
- 32 Schro[®] dinger Release 2018-4: Prime, Schro[®] dinger, LLC, New York, NY, 2018.
- 33 Sastry GM, Adzhigirey M, Day T, Annabhimoju R, Sherman W. Protein and ligand preparation: parameters, protocols, and influence on virtual screening enrichments. *J Comput Aided Mol Des*. 2013;27(3):221–234. <https://doi.org/10.1007/s10822-013-9644-8>.
- 34 Schro[®] dinger Release 2018-4: Protein Preparation Wizard; Epik, Schro[®] dinger, LLC, New York, NY, 2016; Impact, Schro[®] dinger, LLC, New York, NY, 2016; Prime, Schro[®] dinger, LLC, New York, NY, 2018.
- 35 Schro[®] dinger Release 2018-4: LigPrep, Schro[®] dinger, LLC, New York, NY, 2018.
- 36 Friesner RA, Murphy RB, Repasky MP, et al. Extra precision glide: docking and scoring incorporating a model of hydrophobic enclosure for protein-ligand complexes. *J Med Chem*. 2006;49(21):6177–6196. <https://doi.org/10.1021/jm051256o>.
- 37 Halgren TA, Murphy RB, Friesner RA, et al. Glide: a new approach for rapid, accurate docking and scoring. 1. Method and assessment of docking accuracy. *J Med Chem*. 2004; 47(7):1750–1759. <https://doi.org/10.1021/jm030644s>.
- 38 Friesner RA, Banks JL, Murphy RB, et al. Glide: a new approach for rapid, accurate docking and scoring. 1. Method and assessment of docking accuracy. *J Med Chem*. 2004;47(7):1739–1749. <https://doi.org/10.1021/jm0306430>.
- 39 Schro[®] dinger Release 2018-4: Glide, Schro[®] dinger, LLC, New York, NY, 2018.
- 40 Al-Tel TH, Semreen MH, Al-Qawasmeh RA, et al. Design, synthesis, and qualitative structure-activity evaluations of novel β -secretase inhibitors as potential Alzheimer's drug leads. *J Med Chem*. 2011;54(24):8373–8385. <https://doi.org/10.1021/jm201181f>.
- 41 Baviskar AT, Madaan C, Preet R, et al. N-fused imidazoles as novel anticancer agents that inhibit catalytic activity of topoisomerase II α and induce apoptosis in G1/S phase. *J Med Chem*. 2011;54(14):5013–5030. <https://doi.org/10.1021/jm200235u>.
- 42 Gunaganti N, Kharbanda A, Lakkani NR, et al. Catalyst free, C-3 functionalization of imidazo[1,2-a]pyridines to rapidly access new chemical space for drug discovery efforts. *Chem Commun (Camb)*. 2018;54(92):12954–12957. <https://doi.org/10.1039/e8cc07063f>.
- 43 El-Awady RA, Semreen MH, Saber-Ayad MM, Cyprian F, Menon V, Al-Tel TH. Modulation of DNA damage response and induction of apoptosis mediates synergism between doxorubicin and a new imidazopyridine derivative in breast and lung cancer cells. *DNA Repair*. 2016/01/01/ 2016;;37:1–11. <https://doi.org/10.1016/j.dnarep.2015.10.004>.
- 44 Al-Tel TH, Al-Qawasmeh RA, Zaarour R. Design, synthesis and in vitro antimicrobial evaluation of novel imidazo[1,2-a]pyridine and imidazo[2,1-b][1,3]benzothiazole motifs. *Eur J Med Chem*. 2011;46(5):1874–1881. <https://doi.org/10.1016/j.ejmech.2011.02.051>.
- 45 Tarazi H, Odeh RA, Al-Qawasmeh R, Yousef IA, Voelter W, Al-Tel TH. Design, synthesis and SAR analysis of potent BACE1 inhibitors: Possible lead drug candidates for Alzheimer's disease. *Eur J Med Chem*. 2017;125:1213–1224. <https://doi.org/10.1016/j.ejmech.2016.11.021>.
- 46 Lobera M, Madauss KP, Pohlhaus DT, et al. Selective class IIa histone deacetylase inhibition via a nonchelating zinc-binding group. *Nat Chem Biol*. 2013;9(5):319–325. <https://doi.org/10.1038/nchembio.1223>.
- 47 Schroeder FA, Lewis MC, Fass DM, et al. A selective HDAC 1/2 inhibitor modulates chromatin and gene expression in brain and alters mouse behavior in two mood-related tests. *PLoS ONE*. 2013;8(8), e71323. <https://doi.org/10.1371/journal.pone.0071323>.
- 48 Reardon B, Beliakova-Bethell N, Spina CA, et al. Dose-responsive gene expression in suberoylanilide hydroxamic acid-treated resting CD4⁺ T cells. *AIDS (London, England)*. 2015;29(17):2235–2244. <https://doi.org/10.1097/qad.0000000000000839>.
- 49 Miyanaga A, Gemma A, Noro R, et al. Antitumor activity of histone deacetylase inhibitors in non-small cell lung cancer cells: development of a molecular predictive model. *Mol Cancer Ther*. 2008;7(7):1923–1930. <https://doi.org/10.1158/1535-7163.mct-07-2140>.
- 50 El-Awady RA, Hersi F, Al-Tunaiji H, et al. Epigenetics and miRNA as predictive markers and targets for lung cancer chemotherapy. *Cancer Biol Ther*. 2015;16(7): 1056–1070. <https://doi.org/10.1080/15384047.2015.1046023>.
- 51 Hrabeta J, Stiborova M, Adam V, Kizek R, Eckschlager T. Histone deacetylase inhibitors in cancer therapy. A review. *Biomed Pap Med Fac Univ Palacky Olomouc Czech Repub BIOMED PAP* 2014;158(2):161–9. doi: [10.5507/bp.2013.085](https://doi.org/10.5507/bp.2013.085).
- 52 West AC, Johnstone RW. New and emerging HDAC inhibitors for cancer treatment. *J Clin Invest*. 2014;124(1):30–39. <https://doi.org/10.1172/jci69738>.
- 53 Ramadan WS, Vazhappilly CG, Saleh EM, et al. Interplay between Epigenetics, Expression of Estrogen Receptor- α , HER2/ERBB2 and Sensitivity of Triple Negative Breast Cancer Cells to Hormonal Therapy. *Cancers (Basel)* 2018;11(1). doi: [10.3390/cancers11010013](https://doi.org/10.3390/cancers11010013).
- 54 Suzuki J, Chen YY, Scott GK, et al. Protein acetylation and histone deacetylase association associated with malignant breast cancer progression. *Clin Cancer Res*. 2009;15(9):3163–3171. <https://doi.org/10.1158/1078-0432.ccr-08-2319>.
- 55 Krusche CA, Wülfing P, Kersting C, et al. Histone deacetylase-1 and -3 protein expression in human breast cancer: a tissue microarray analysis. *Breast Cancer Res Treat*. 2005;90(1):15–23. <https://doi.org/10.1007/s10549-004-1668-2>.
- 56 Müller BM, Jana L, Kasajima A, et al. Differential expression of histone deacetylases HDAC1, 2 and 3 in human breast cancer-overexpression of HDAC2 and HDAC3 is associated with clinicopathological indicators of disease progression. *BMC Cancer*. 2013;13:215. <https://doi.org/10.1186/1471-2407-13-215>.
- 57 Hebach C, Kallen EJ, Ternois James GJ, intelnot-Blomley M. Novel trifluoromethyl-oxadiazole derivatives and their use in the treatment of disease. 2013; WO/2013/008162.
- 58 Hu Z, Wang J. Histone deacetylase inhibitor induces the expression of select epithelial genes in mouse utricle sensory epithelia-derived progenitor cells. *Cell Reprogram*. 2014;16(4):266–275. <https://doi.org/10.1089/cell.2013.0086>.
- 59 Karbownik MS, Szemraj J, Wieteska L, et al. Antipsychotic Drugs Differentially Affect mRNA Expression of Genes Encoding the Neuregulin 1-Downstream ErbB4-P13K Pathway. *Pharmacology*. 2016;98(1-2):4–12. <https://doi.org/10.1159/000444534>.
- 60 Pu M, Ni Z, Wang M, et al. Trimethylation of Lys36 on H3 restricts gene expression change during aging and impacts life span. *Genes Dev*. 2015;29(7):718–731. <https://doi.org/10.1101/gad.254144.114>.
- 61 Liu T, Liu P, Marshall G. The Critical Role of the Class III Histone Deacetylase SIRT1 in Cancer. *Cancer Res*. 2009;69(5):1702–1705. <https://doi.org/10.1158/0008-5472.CAN-08-3365>.
- 62 Balli P, Pranpat M, Swaby R, et al. Activity of suberoylanilide hydroxamic Acid against human breast cancer cells with amplification of her-2. *Clin Cancer Res*. 2005; 11(17):6382–6389. <https://doi.org/10.1158/1078-0432.ccr-05-0344>.
- 63 Drogaris P, Villeneuve V, Pomi^{es} C, et al. Histone deacetylase inhibitors globally enhance h3/h4 tail acetylation without affecting h3 lysine 56 acetylation. *Sci. Rep*. 2012;2:220–220. doi: [10.1038/srep00220](https://doi.org/10.1038/srep00220).
- 64 Tate CR, Rhodes LV, Segar HC, et al. Targeting triple-negative breast cancer cells with the histone deacetylase inhibitor panobinostat. *Breast Cancer Res*. 2012;14(3): R79. <https://doi.org/10.1186/bcr3192>.
- 65 Hsu KW, Huang CY, Tam KW, et al. The Application of Non-Invasive Apoptosis Detection Sensor (NIADS) on Histone Deacetylation Inhibitor (HDACi)-Induced Breast Cancer Cell Death. *Int J Mol Sci*. 2018;19(2). [10.3390/ijms19020452](https://doi.org/10.3390/ijms19020452).
- 66 Zhao H, Wang W, Zhao Q, Hu G, Deng K, Liu Y. BCL3 exerts an oncogenic function by regulating STAT3 in human cervical cancer. *Oncol Targets Ther*. 2016;9:6619–6629. <https://doi.org/10.2147/ott.s118184>.
- 67 Herrington FD, Nibbs RJB. Regulation of the Adaptive Immune Response by the I κ B Family Protein Bcl-3. *Cells*. 2016;5(2):14. <https://doi.org/10.3390/cells5020014>.
- 68 Kiweler N, Wünsch D, Wirth M, et al. Histone deacetylase inhibitors dysregulate DNA repair proteins and antagonize metastasis-associated processes. *J Cancer Res Clin Oncol*. 2020;146(2):343–356. <https://doi.org/10.1007/s00432-019-03118-4>.
- 69 Lee YJ, Won AJ, Lee J, et al. Molecular mechanism of SAHA on regulation of autophagic cell death in tamoxifen-resistant MCF-7 breast cancer cells. *Int J Med Sci*. 2012;9(10):881–893. <https://doi.org/10.7150/ijms.5011>.
- 70 Munster PN, Trosco-Sandoval T, Rosen N, Rifkind R, Marks PA, Richon VM. The histone deacetylase inhibitor suberoylanilide hydroxamic acid induces differentiation of human breast cancer cells. *Cancer Res*. 2001;61(23):8492–8497.
- 71 Kuo SJ, Lin HY, Chien SY, Chen DR. SIRT1 suppresses breast cancer growth through downregulation of the Bcl-2 protein. *Oncol Rep*. 2013;30(1):125–130. <https://doi.org/10.3892/or.2013.2470>.
- 72 Alao JP, Lam EW, Ali S, et al. Histone deacetylase inhibitor trichostatin A represses estrogen receptor alpha-dependent transcription and promotes proteasomal degradation of cyclin D1 in human breast carcinoma cell lines. *Clin Cancer Res*. 2004; 10(23):8094–8104. <https://doi.org/10.1158/1078-0432.ccr-04-1023>.